

POLITECNICO DI TORINO

Facoltà di Ingegneria Meccanica e Aerospaziale
Corso di Laurea in Aerospace Engineering

Tesi di Laurea

**Characterization of mechanical
properties of 3D printed
continuous carbon fiber reinforced
composites**

Relatori:

prof. Carrera Erasmo, prof. Montemurro Marco
dott. Pagani Alfonso, dott.ssa Catapano Anita
dott. Zappino Enrico, dott. Panettieri Enrico

Candidato:

Micali Lorenzo

Luglio 2018

Acknowledgments

I would first like to thank my thesis advisor Prof. Erasmo Carrera of the Mechanical and Aerospace Department at Politecnico di Torino to have the opportunity to complete my work "Characterization of mechanical properties of 3D printed continuous carbon fiber reinforced composites".

I would also like to thank the professors who were involved in the validation survey for this research project: Prof. Alfonso Pagani and Prof. Enrico Zappino. Without their passionate participation and input, the validation survey could not have been successfully conducted. The door to Prof. Pagani office was always open whenever I ran into a trouble spot or had a question about my research or writing. They consistently allowed this paper to be my own work, but steered me in the right the direction whenever he thought I needed it.

I would like to thank my thesis advisors in Bordeaux Prof. Marco Montemurro and Prof. Anita Catapano of the Mechanical and Engineering Research Institute I2M at ENSAM Art et Metiers ParisTech.

I would also like to acknowledge Dr. Enrico Panettieri and Dr. Michele Jacopo Izzi who followed constantly this work during the period spent in Bordeaux. I am gratefully indebted to them for their very valuable comments on this thesis. Their guidance helped me during the time of research in Bordeaux.

Finally, I must express my very profound gratitude to my father for providing me with unfailing support and continuous encouragement throughout my years of study and through the process of researching and writing this thesis. This accomplishment would not have been possible without him. Thank you.

Lorenzo Micali

Summary

This thesis presents a characterization of mechanical properties of 3D printed continuous carbon fiber reinforced composites.

This work has been realized through additive manufactured material using fused deposition modelling technique.

Materials used were Nylon and Carbon fiber reinforced.

Manufacturing was performed using Markforged's - Mark Two 3D printer, importing STL files from the CAD SolidWorks.

Different samples with varying infill patterns were printed and tested and results indicate an isotropic behavior through the manufactured samples.

It has been analyzed the influence of strain rate and aging on the samples, influencing consistently the sigma-epsilon graphs.

Traction experiments and three point bending tests were performed.

The aim of this study is to evaluate the elastic properties of the nylon and the fiber reinforced 3D printed structures following ASTM norms.

The study is done in collaboration with ENSAM - Arts et Metiers ParisTech Bordeaux, where traction tests and three point bending tests have been performed.

Post-processing analysis has been developed through digital image correlation data, in order to find the Poisson's ratio and the shear modulus of each sample.

Table of contents

Acknowledgments	I
Summary	II
1 Introduction	1
1.1 Backgrounds	1
1.2 Motivation	1
1.3 Objective	2
1.4 Methodology	2
2 Additive manufacturing	4
2.1 Main process methods	4
2.1.1 Vat Photopolymerisation	4
2.1.2 Material Jetting	5
2.1.3 Binder Jetting	7
2.1.4 Material Extrusion	7
2.1.5 Powder Bed Fusion	9
2.1.6 Sheet Lamination	10
2.1.7 Directed Energy Deposition	11
2.2 ATL and AFP	12
2.2.1 ATL - Automated Tape Laying	13
2.2.2 AFP - Automated Fibre Placement	14
2.3 Variable Angle Tow Composites	15
2.3.1 Limitations of fibre placement techniques for VAT Composites	16
2.4 Aerospace Applications	16
3 Normatives	18
3.1 ASTM	18
3.1.1 D638 Plastics	18
3.1.2 D3039 Reinforced Composites	20

3.1.3	D790 Flexural Properties of Unreinforced and Reinforced Plastics and Electrical Insulating Materials	22
3.2	Applicability of current normatives to additive manufacturing of composites structures	23
3.3	State of art - Current literature	25
4	Preparation for testing	26
4.1	Markforged 3D Printing	26
4.2	Samples Manufacturing	29
4.2.1	Nylon specimens	30
4.2.2	Carbon Fiber specimens	31
4.2.3	Carbon Fiber plates	34
4.3	Dimensional accuracy	35
4.3.1	Nylon	36
4.3.2	Carbon Fiber	37
4.3.3	Comparison between Dimensions Norms - Reality	39
4.4	Microscopic measurements	40
5	Traction test	44
5.1	Sigma-epsilon graphs	45
5.1.1	Nylon and Carbon fiber compared between Standard velocities	46
5.1.2	Influence of strain rate	51
5.1.3	Influence of aging	53
5.2	Young Modulus	54
5.2.1	Nylon	55
5.2.2	Carbon fiber	56
6	Three point bending test	59
6.1	Sigma-epsilon graphs	61
6.2	Young modulus	62
7	Digital image correlation	64
7.1	Poisson's ratio and Shear modulus	65
7.1.1	Nylon	66
7.1.2	Carbon Fiber	70
8	Conclusions	75
	Bibliography	76

List of figures

1.1	Additive Manufacturing Time History.	2
2.1	Scheme of VAT Process.	5
2.2	Scheme of Material Jetting Process.	6
2.3	Scheme of Binder Jetting Process.	7
2.4	Scheme of Material Extrusion Process.	8
2.5	Scheme of Powder Bed Fusion Process.	10
2.6	Scheme of Sheet Lamination Process.	11
2.7	Scheme of Directed Energy Deposition Process.	12
2.8	Scheme of Automated Tape Laying.	13
2.9	Scheme of Automated Fibre Placement.	14
2.10	VAT Composites.	15
3.1	ASTM Specimen for Plastics.	19
3.2	ASTM Specimen Dimensions for Plastics.	19
3.3	ASTM Specimen geometry for Composites.	20
3.4	ASTM Specimen dimensions for Composites.	21
3.5	Reference picture, strain gage and specimen dimensions in scale.	21
3.6	Three-point bending.	22
4.1	Markforged - Mark Two 3D printer.	26
4.2	Unidirectional and $\pm 45^\circ$ rectangular infill pattern.	27
4.3	Triangular infill pattern.	28
4.4	Setup before printing.	28
4.5	Nylon sample CAD.	29
4.6	Carbon fiber sample CAD for traction test.	30
4.7	Nylon samples.	30
4.8	Software internal view of a hexagonal pattern.	31
4.9	Software internal view of a triangular pattern.	31
4.10	Carbon Fiber samples.	32
4.11	NC0125F2W1D0 Software internal view.	32
4.12	NC0125F4W1D90 Software internal view.	33

4.13	0 ° carbon fiber specimens for 3pb test.	34
4.14	0 ° carbon fiber plate.	34
4.15	Water jet cutter.	35
4.16	Plan view of the sample section.	35
4.17	Average Areas for each batch of Nylon samples.	36
4.18	Average Areas for each batch of Carbon fiber samples.	37
4.19	Average Areas for each batch of 3pb Carbon fiber samples.	38
4.20	Microscope lens.	40
4.21	Width of attached Carbon Fibers.	41
4.22	Fiber sections.	41
4.23	Single Fiber width.	42
4.24	Fibers detail.	42
4.25	Composite Fracture.	43
4.26	Lamination.	43
4.27	Lateral view lamination.	43
5.1	Traction test setup.	44
5.2	Carbon fiber specimen after traction test.	45
5.3	Rectangular Nylon N02R100F10.	46
5.4	Rectangular Nylon N02R50F4.	47
5.5	Hexagonal Nylon N02H50F4.	47
5.6	Triangular Nylon N02T25F4.	48
5.7	Triangular Nylon N02T50F4.	48
5.8	Triangular Nylon N02T75F4.	49
5.9	Carbon fiber NC0125F2W1D0.	49
5.10	Carbon fiber NC0125F3W2D0.	50
5.11	Carbon fiber NC0125F4W1D90.	51
5.12	Carbon fiber NC0125F1W1D0.	51
5.13	Different velocities of Nylon N02R100F10.	52
5.14	Different velocities of Nylon N02R50F4.	52
5.15	Different velocities of Nylon N02H50F4.	53
5.16	Old and new samples of Nylon N02R100F10.	54
5.17	Old and new samples of Nylon N02R50F4.	54
5.18	E_{Total} variation with different patterns.	56
5.19	E Variation with different density.	57
5.20	Carbon fiber E Variation.	58
6.1	Three-point bending setup.	59
6.2	Three-point bending setup.	60
6.3	Sigma-epsilon graph of carbon fiber samples for 3pb.	61
6.4	Sigma-epsilon graph of only carbon fiber for 3pb.	62

7.1	Setup for digital image correlation.	64
7.2	G modulus.	66
7.3	$\epsilon_y - \epsilon_x$ graph of third and fourth Nylon N02R100F10 sample.	67
7.4	Photo of Nylon N02R100F10.3 before and after traction.	67
7.5	Tangential Strain for nylon N02R100F10.3.	68
7.6	Tangential Strain long x axis for Nylon N02R100F10.4.	68
7.7	$\epsilon_y - \epsilon_x$ graph of the fifth Nylon N02T25F4 and N02T25F4 sample.	69
7.8	Photo of Nylon N02T25F4.5 before and after traction.	69
7.9	Tangential Strain for N02T25F4.5.	69
7.10	Strain vs time.	70
7.11	$\epsilon_y - \epsilon_x$ graph of NC0125F2W1D0.1 and NC0125F3W2D0.1.	71
7.12	Photo of Carbon Fiber NC0125F2W1D0.1 before and after traction.	72
7.13	Photo of Carbon Fiber NC0125F4W1D90.1 before and after traction.	72
7.14	$\epsilon_y - \epsilon_x$ graph of Carbon Fiber NC0125F4W1D90.1.	73
7.15	Tangential Strain for NC0125F4W1D90.1.	73
7.16	NC0125F1W1D0.3 ϵ_x graph.	74
7.17	NC0125F1W1D0 Poisson's ratio.	74

List of tables

2.1	Advantages and Disadvantages of VAT Photopolymerisation.	5
2.2	Advantages and Disadvantages of Material Jetting.	6
2.3	Advantages and Disadvantages of Binder Jetting.	8
2.4	Advantages and Disadvantages of Material Extrusion.	9
2.5	Advantages and Disadvantages of Powder Bed Fusion.	9
2.6	Advantages and Disadvantages of Sheet Lamination.	11
2.7	Advantages and Disadvantages of Directed Energy Deposition.	12
2.8	Advantages and Disadvantages of ATL.	14
3.1	Standards Applicability Assessment.	24
4.1	Markforged parameters.	27
4.2	Sample codes.	29
4.3	Carbon fiber samples part settings for traction test.	32
4.4	Carbon fiber samples part settings for 3pb.	33
4.5	Nylon Width and Thickness Averages.	36
4.6	Carbon Fiber Width and Thickness Averages.	37
4.7	NC0125F1W1D0 layers composition.	38
4.8	Volume Percentage of Nylon Samples.	39
4.9	Volume Percentage of Carbon fiber Samples.	39
5.1	Nylon Young's modulus calculation.	55
5.2	Carbon fiber Young's modulus calculation.	56
6.1	Carbon fiber Young's modulus calculation for 3pb.	63
7.1	Poisson's ratio and Shear modulus of nylon samples.	66
7.2	Poisson's ratio and Shear modulus of carbon fiber samples.	71

Chapter 1

Introduction

1.1 Backgrounds

The additive manufacturing (AM) obtained large diffusion in the 2000s, inspired by the theme of material being added together. The term 3D printing still referred only to the polymer technologies in most minds, and the term AM was likelier to be used in metalworking and end-use part production contexts.

By the early 2010s, the terms 3D printing and additive manufacturing evolved alternating each other in the AM technologies world, one being used via media by consumer-maker communities, and the other used more formally by industrial AM end-use part producers, AM machine manufacturers, and global technical standards organizations. Other terms that have been used as AM synonyms have included desktop manufacturing, rapid manufacturing, and on-demand manufacturing.

Additive manufacturing processes take the information from a computer-aided design (CAD) file that is later converted to a stereolithography (STL) file. In this process, the drawing made in the CAD software is approximated by triangles and sliced containing the information of each layer that is going to be printed.

The aerospace industry employs AM because of the possibility of manufacturing lighter structures to reduce weight.

1.2 Motivation

The work presented in this thesis is in collaboration with ENSAM - Art et Metiers ParisTech in Bordeaux. In recent years, additive manufacturing has gained a lot of interest of the industry as a good addition to more traditional manufacturing techniques. The gained interest results in highly optimized products using less material, reduction in both printing time and energy consumed during printing. Even if the manufacturing technique where introduced in the 1980s, a good tool to

predict the final properties of the material is still missing.

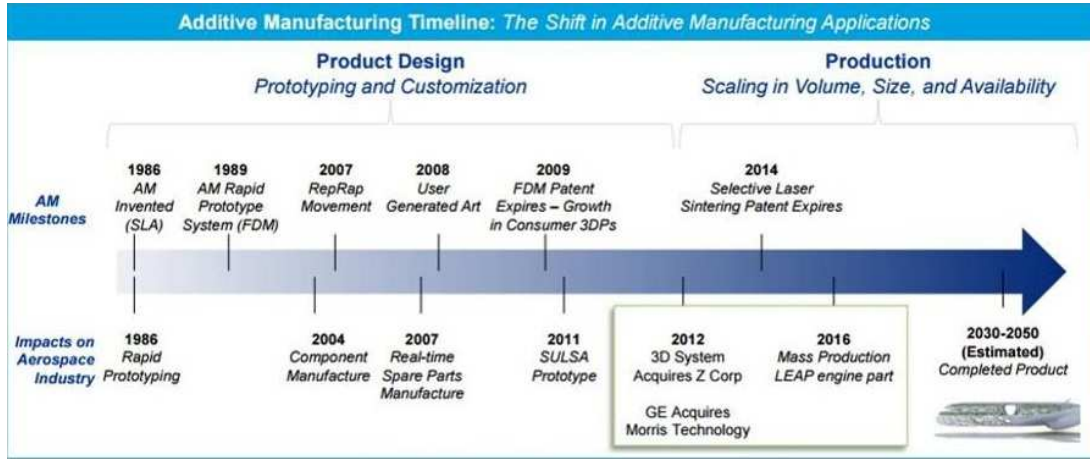


Figure 1.1. Additive Manufacturing Time History.

1.3 Objective

In this project the objective is to investigate the mechanical properties of 3D printed continuous carbon fiber reinforced composites.

In this work it has been performed a lot of tests in order to find a trend in additive manufacturing between manufacturing tool path, traction of the material and the final mechanical properties. If there is, conclusions can be drawn on how the results are different or similar compared to datasheet given by the software Eiger of the 3D - printer Markforged Two. An internal pattern is implemented to find anisotropic or isotropic behaviour on the mechanical properties. Shape distortion will be measured on samples with different infill percentage, geometry and infill pattern. The intention is to find trends in shape distortion based on these different configurations. Additional mechanical testing is aimed to link the mechanical behaviour to the magnitude of shape distortion.

1.4 Methodology

To reach the objectives in this thesis work, the material and its environment are characterized. Experiments are performed separately on each specimen types. Internal patterns are implemented with varying geometry, infill percentage and infill pattern. To measure shape distortion each sample is scanned and compared to its

CAD geometry. Each sample is also measured to confirm the reliability of the input data such as infill percentage. Investigating the trends in volume difference on each parameter, optimized configurations will be found to minimize shape distortion. Each sample is also traction tested to find the traction properties in axial directions.

Chapter 2

Additive manufacturing

2.1 Main process methods

The first form of creating layer by layer a three dimensional object using computer aided design (CAD) was rapid prototyping, developed in the 1980s for creating models and prototype parts. [1] [2] Rapid prototyping is one of the earlier additive manufacturing (AM) processes. It allows for the creation of printed parts, not just models. Among the major advances that this process presented to product development are the time and cost reduction, human interaction, and consequently the product development cycle, also the possibility to create almost any shape that could be very difficult to machine.

Nowadays, the technologies of rapid prototyping are not just used for creating models, with the advantages in plastic materials it has been possible to create finished products. [3] In addition, it is important to notice that rapid manufacturing became possible by other technologies, which are computer-aided design (CAD), computer-aided manufacturing (CAM), and computer numerical control (CNC). Those three technologies combined made possible the printing of three-dimensional objects. [4]

2.1.1 Vat Photopolymerisation

Vat polymerisation uses a vat of liquid photopolymer resin, out of which the model is constructed layer by layer. An ultraviolet (UV) light is used to cure or harden the resin where required, while a platform moves the object being made downwards after each new layer is cured.

The main steps of photopolymerisation are:

- The build platform is lowered from the top of the resin vat downwards by the layer thickness.
- A UV light cures the resin layer by layer. The platform continues to move downwards and additional layers are built on top of the previous.

- Some machines use a blade which moves between layers in order to provide a smooth resin base to build the next layer on.
- After completion, the vat is drained of resin and the object removed.

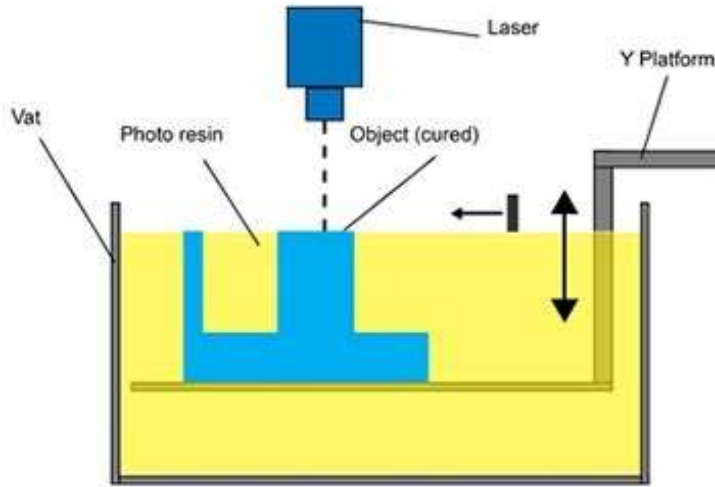


Figure 2.1. Scheme of VAT Process.

VAT Photopolymerisation	
<i>Advantages</i>	<i>Disadvantages</i>
<ul style="list-style-type: none"> - High level of accuracy - Relatively quick process - Typically large build areas 	<ul style="list-style-type: none"> - Relatively expensive - Lengthly post processing time - Limited material use - Requires support structures

Table 2.1. Advantages and Disadvantages of VAT Photopolymerisation.

2.1.2 Material Jetting

Material jetting creates objects in a similar method to a two dimensional ink jet printer. Material is jetted onto a build platform using either a continuous or Drop on Demand (DOD) approach.

Material is jetted onto the build surface or platform, where it solidifies and the model is built layer by layer. Material is deposited from a nozzle which moves

horizontally across the build platform. Machines vary in complexity and in their methods of controlling the deposition of material. The material layers are then cured or hardened using ultraviolet (UV) light.

The main steps of material jetting are:

- The print head is positioned above build platform.
- Droplets of material are deposited from the print head onto surface where required, using either thermal or piezoelectric method.
- Droplets of material solidify and make up the first layer.
- Further layers are built up as before on top of the previous.
- Layers are allowed to cool and harden or are cured by UV light. Post processing includes removal of support material.

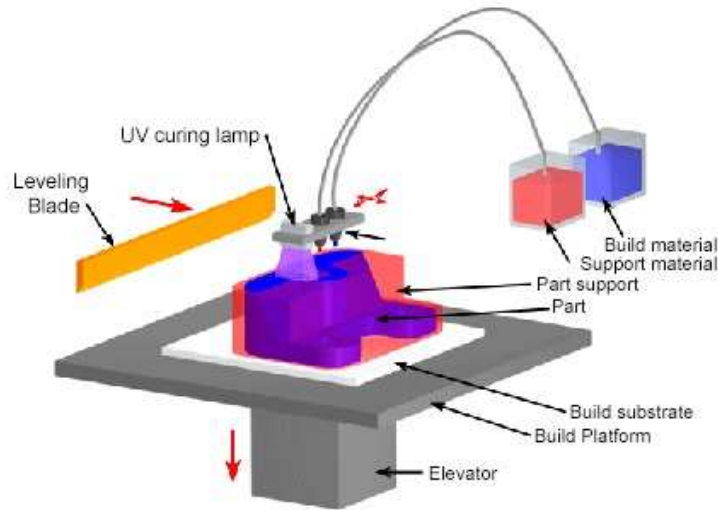


Figure 2.2. Scheme of Material Jetting Process.

Material Jetting	
<i>Advantages</i>	<i>Disadvantages</i>
<ul style="list-style-type: none"> - High accuracy of deposition - Multiple parts under one process 	<ul style="list-style-type: none"> - Support material required - Limited materials

Table 2.2. Advantages and Disadvantages of Material Jetting.

2.1.3 Binder Jetting

The binder jetting process uses two materials; a powder based material and a binder. The binder acts as an adhesive between powder layers. The binder is usually in liquid form and the build material in powder form. A print head moves horizontally along the x and y axes of the machine and deposits alternating layers of the build material and the binding material. After each layer, the object being printed is lowered on its build platform.

The main steps of Binder Jetting are:

- Powder material is spread over the build platform using a roller.
- The print head deposits the binder adhesive on top of the powder where required.
- The build platform is lowered by the model's layer thickness.
- Another layer of powder is spread over the previous layer. The object is formed where the powder is bound to the liquid.
- Unbound powder remains in position surrounding the object.
- The process is repeated until the entire object has been made.

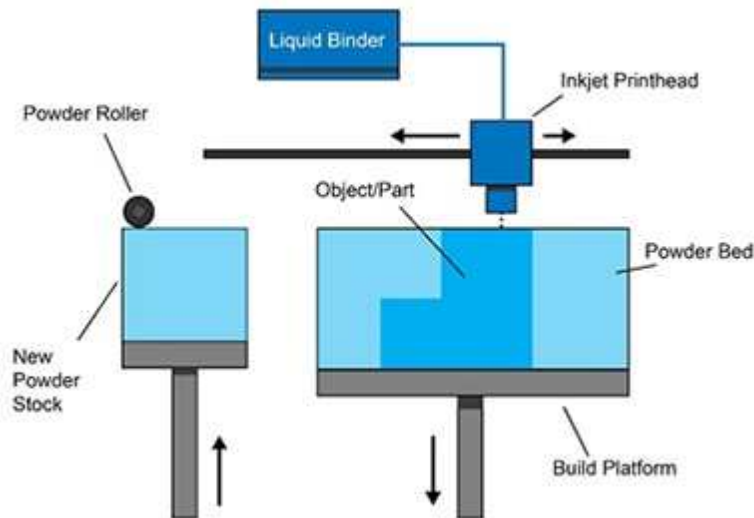


Figure 2.3. Scheme of Binder Jetting Process.

2.1.4 Material Extrusion

Fuse deposition modelling (FDM) [5] is a common material extrusion process and is trademarked by the company Stratasys. Material is drawn through a nozzle, where

Binder Jetting

<i>Advantages</i>	<i>Disadvantages</i>
- Range of different colours	- Not suitable for structural parts
- Different range of materials	- Post processing add time to the process
- The process is faster than others	

Table 2.3. Advantages and Disadvantages of Binder Jetting.

it is heated and is then deposited layer by layer. The nozzle can move horizontally and a platform moves up and down vertically after each new layer is deposited.

The main steps of material extrusion are:

- First layer is built as nozzle deposits material where required onto the cross sectional area of first object slice.
- The following layers are added on top of previous layers.
- Layers are fused together upon deposition as the material is in a melted state.

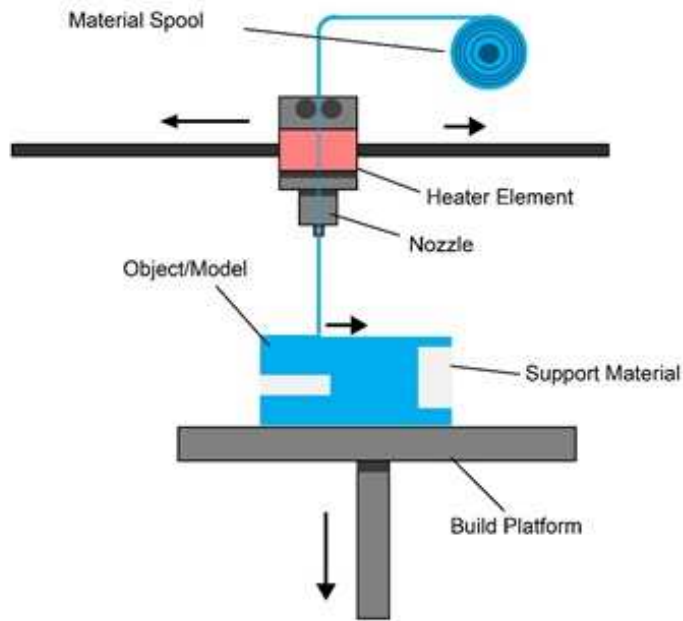


Figure 2.4. Scheme of Material Extrusion Process.

Material Extrusion	
<i>Advantages</i>	<i>Disadvantages</i>
- Widespread and inexpensive process	- The nozzle radius limits the quality
- ABS plastic can be used	- Accuracy lower than other processes

Table 2.4. Advantages and Disadvantages of Material Extrusion.

2.1.5 Powder Bed Fusion

The Powder Bed Fusion process includes the following commonly used printing techniques: Direct metal laser sintering (DMLS), Electron beam melting (EBM), Selective heat sintering (SHS), Selective laser melting (SLM) and Selective laser sintering (SLS).

Powder bed fusion (PBF) methods use either a laser or electron beam to melt and fuse material powder together. Electron beam melting (EBM), methods require a vacuum but can be used with metals and alloys in the creation of functional parts. Direct metal laser sintering (DMLS) is the same as SLS, but with the use of metals and not plastics. The process sinters the powder, layer by layer. Selective Heat Sintering (SHS) differs from other processes by way of using a heated thermal print head to fuse powder material together. As before, layers are added with a roller in between fusion of layers. A platform lowers the model accordingly.

The main steps of powder bed fusion are:

- A layer, typically 0.1mm thick of material is spread over the build platform.
- A laser fuses the first layer or first cross section of the model.
- A new layer of powder is spread across the previous layer using a roller.
- Further layers or cross sections are fused and added.
- The process repeats until the entire model is created. Loose, unfused powder is remains in position but is removed during post processing.

Powder Bed Fusion	
<i>Advantages</i>	<i>Disadvantages</i>
- Relatively inexpensive	- Relatively slow speed (SHS)
- Suitable for visual models	- Lack of material structural properties
- Ability to integrate into small scale	- Size limitations
- Powder acts as integrated structure	- High power usage
- Large range of material options	- Finish depending on powder grain size

Table 2.5. Advantages and Disadvantages of Powder Bed Fusion.

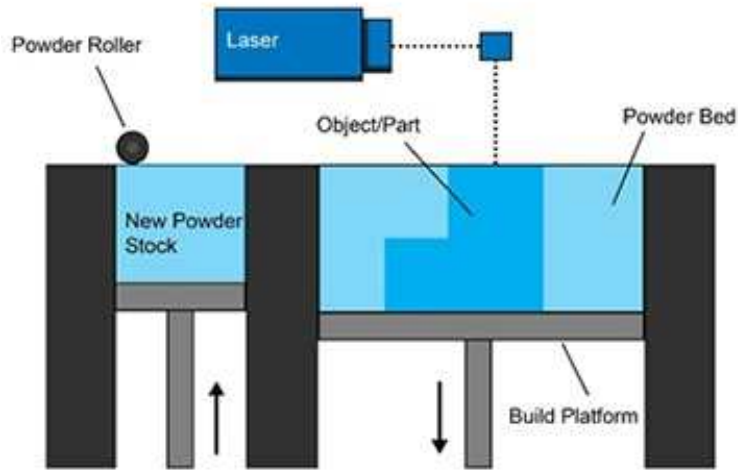


Figure 2.5. Scheme of Powder Bed Fusion Process.

2.1.6 Sheet Lamination

Sheet lamination processes include ultrasonic additive manufacturing (UAM) and laminated object manufacturing (LOM). The Ultrasonic Additive Manufacturing process uses sheets or ribbons of metal, which are bound together using ultrasonic welding. The process does require additional cnc machining and removal of the unbound metal, often during the welding process. Laminated object manufacturing (LOM) uses a similar layer by layer approach but uses paper as material and adhesive instead of welding.

The main steps of sheet lamination are:

- The material is positioned in place on the cutting bed.
- The material is bonded in place, over the previous layer, using the adhesive.
- The required shape is then cut from the layer, by laser or knife.
- The next layer is added.
- Steps two and three can be reversed and alternatively, the material can be cut before being positioned and bonded.

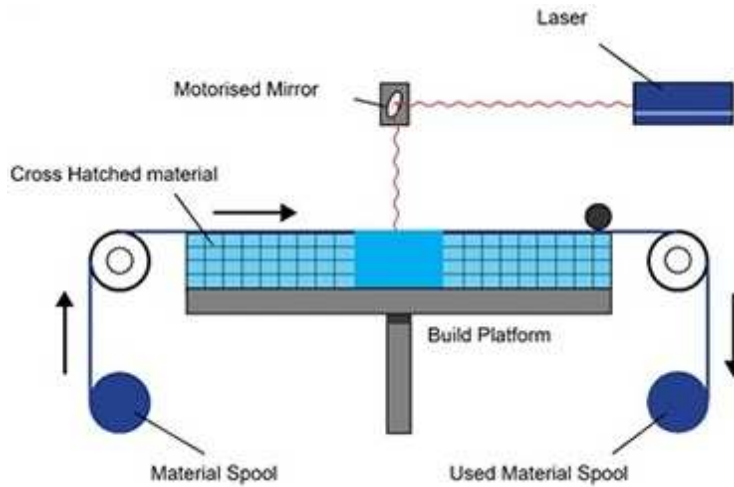


Figure 2.6. Scheme of Sheet Lamination Process.

Sheet Lamination

Advantages

- Speed, low cost
- Cutting is fast due to cutting route

Disadvantages

- Finishes depending on plastic material
 - Limited material use
-

Table 2.6. Advantages and Disadvantages of Sheet Lamination.

2.1.7 Directed Energy Deposition

Directed Energy Deposition (DED) covers a range of terminology: 'Laser engineered net shaping, directed light fabrication, direct metal deposition, 3D laser cladding'. It is a more complex printing process commonly used to repair or add additional material to existing components.

A typical DED machine consists of a nozzle mounted on a multi axis arm, which deposits melted material onto the specified surface, where it solidifies. The process is similar in principle to material extrusion, but the nozzle can move in multiple directions and is not fixed to a specific axis.

The main steps of direct energy deposition are:

- A4 or 5 axis arm with nozzle moves around a fixed object.
- Material is deposited from the nozzle onto existing surfaces of the object.
- Material is either provided in wire or powder form.
- Material is melted using a laser, electron beam or plasma arc upon deposition.
- Further material is added layer by layer and solidifies, creating or repairing new material features on the existing object.

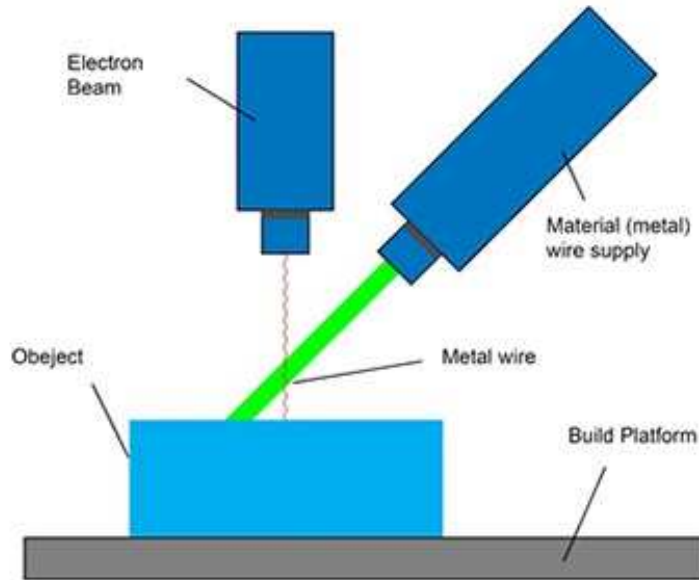


Figure 2.7. Scheme of Directed Energy Deposition Process.

Directed Energy Deposition	
<i>Advantages</i>	<i>Disadvantages</i>
- Advantages of DED	- Finishes depending on plastic material
- Control structure to high degree	- Limited material use
- Balance between quality and speed	- Fusion processes require research

Table 2.7. Advantages and Disadvantages of Directed Energy Deposition.

2.2 ATL and AFP

Highly consistent quality and cost-effective manufacture of advanced composites can be achieved through automation. It may therefore open up new markets and applications for composite products in aerospace, automotive, renewable energy, and consumer goods. Automated Tape Laying (ATL) and Automated Fibre Placement (AFP) are the two main technologies used to automate the layup of prepreg. The state of the art for both technologies is described and current gaps in the understanding of both processes highlighted.

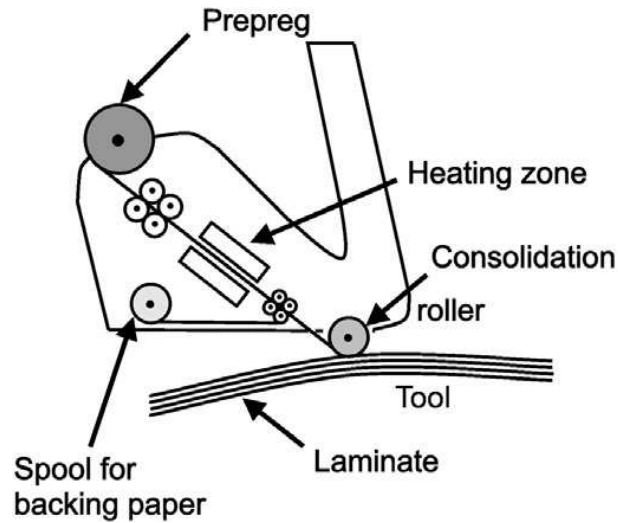


Figure 2.8. Scheme of Automated Tape Laying.

2.2.1 ATL - Automated Tape Laying

Tape heating was introduced in the 1990s to overcome issues during layup of complex laminates, and enable tack control for layup of large parts. ATL can be considered a highly productive process for prepreg layup, which is in widespread use in the aerospace and renewable energy industries.

In Table 2.8 are reported the advantages and the disadvantages of this technology. Despite the potential complexity limitations of ATL manufacture, it has recently received renewed interest due to the high productivity achievable for flat laminates. After layup, flat laminates can be formed into the desired shape by hot drape forming, offering a cost competitive manufacturing route for large composite components and material with high prepreg areal weight, however forming may detrimentally affect the mechanical performance of the structure.

At the start of a layup sequence, the ATL system attaches a predetermined length of tape onto the tool using a soft silicone roller. Once the course has been applied, the system accelerates to the layup speed and delivers the remaining material. During layup the material is attached to the tooling using controlled additional force that is transferred through the end-effector. To control the temperature during layup the material can be heated either in front of the layup head or on the layup system in delivery. At the end of the ply course the head decelerates just prior to finishing and cuts the tape automatically, using rotating or pinching blades.

This entire process is repeated course by course until the ply is finished, the system is stopped by the program, user intervention, or if an automated fault detection system has identified a layup error.

ATL	
<i>Advantages</i>	<i>Disadvantages</i>
- High layup rates	- High initial capital expenditure
- High mechanical properties	- Limited geometric complexity capability
- Manufacture large parts	- Higher material wastage rates than AFP
- Handle high weight materials	

Table 2.8. Advantages and Disadvantages of ATL.

2.2.2 AFP - Automated Fibre Placement

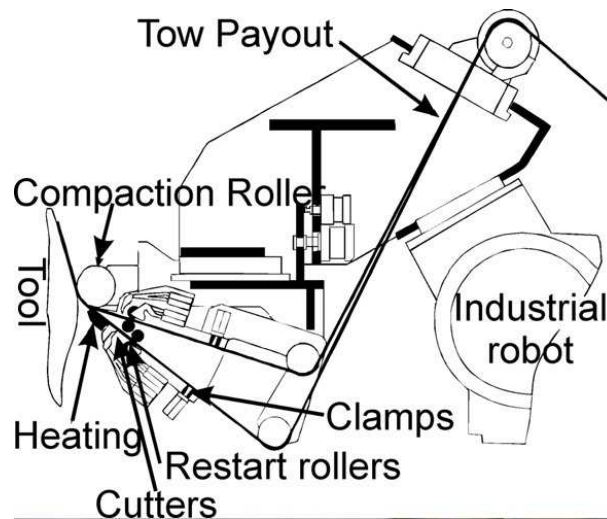


Figure 2.9. Scheme of Automated Fibre Placement.

AFP systems were commercially introduced towards the end of the 1980s, and were described as a logical combination of ATL and Filament winding (FW); by combining the differential payout capability of FW and the compaction and cut-restart capability of ATL.

The AFP system controlled layup speed, pressure, temperature, and tape tension. Layup accuracy is highly important for AFP because the narrow tape will result in gaps between the material, which are a function of the placement accuracy, and may affect mechanical performance.

AFP process systems differ from ATL in the width of the material that is laid down with typical material widths. Each tow is normally driven individually and can be clamped, cut, and restarted, during manufacture. This makes it possible to deliver each tow at individual speeds, enabling layup over complex geometries and some tow

steering. The composite material for AFP layup can either be impregnated tows or slit prepreg tape. Despite the differences in material form and material supply to the layup head, the layup operation during AFP is like that of ATL.

2.3 Variable Angle Tow Composites

The use of the AFP technology brought to the emergence of a new class of composite materials: the variable angle tow (VAT) composites. [6] A modern AFP machine allows the fiber to be placed along a curvilinear path within the constitutive lamina thus implying a point-wise variation of the material properties.

Of course, this technology enables the designer to take advantage of the directional properties of composites in the most effective way. The complexity of the design process of a VAT laminated structure is mainly due to two intrinsic properties of VAT composites, i.e. the heterogeneity and the anisotropy that intervene at different scales of the problem and that vary point-wise over the structure.

[7] The structural efficiency of composite panels with tailored fibre paths has attracted great attention in recent decades. It was proved analytically that tailoring of the in-plane stiffness of composite laminates can improve the buckling and post-buckling characteristics by redistributing the applied loads.

[8] [9] [10] [11] In Fig. 2.10 it shows a photo of VAT composites with different types of internal curves.

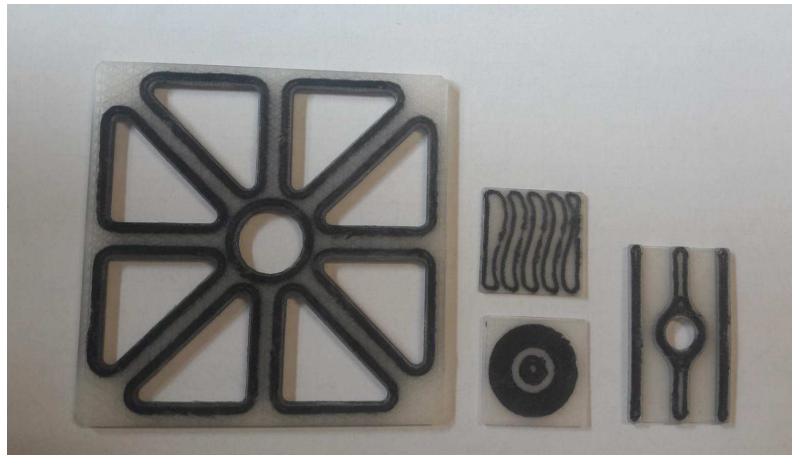


Figure 2.10. VAT Composites.

2.3.1 Limitations of fibre placement techniques for VAT Composites

Currently, there is significant interest in developing methodologies to design optimal fibre orientations for maximizing the structural efficiency.

[12] The fibre placement technique is the core technology underpinning variable stiffness composites. The automated fibre placement techniques can be distinguished by the status of fibre. Pre-impregnated fibre bundles, i.e. towpreg or slittape, have widely been used previously. Recently some researchers have attempted to use the dry fibre bundle to overcome the disadvantages of the tape placement and increase the design flexibility of the variable stiffness composite.

Through the technical review on the conventional wet and dry tow placement techniques, it was found that the key factor causing all process-induced defects was the in-plane bending deformation of the tow. Especially in the shifting method, all defects such as tow gap, tow overlap, fibre misalignment and irregular thickness distribution were come from this fundamental principle of the conventional method. Also, it significantly decreased design flexibility by limiting the minimum radius of curvature of each tow path.

As a novel way of solving these problems, a method using the in-plane shear deformation of the tow can be used with dry tows. Although the thickness change according to the shear deformation is inevitable, the thickness uniformity can be much superior to that of the conventional method using tow drop, tow overlap and staggering to dilute the irregularity of the thickness distribution. Consequently, this continuous shearing method using a dry tow will be a main stream of the future composite manufacturing technology.

2.4 Aerospace Applications

With additive manufacturing technologies it is possible to manufacture lightweight parts. [13] In the aerospace industry the main goal is to make the lightest practical aircraft while securing safety. Additive manufacturing technologies have enabled the manufacture of complex cross-sectional areas like the honeycomb cell or every other material part that contains cavities and cut-outs which reduce the weight-strength relation.

Selective laser sintering, and electron beam are now used in the aircraft and aerospace industries. Engineers perform design within the manufacturing constrains but this process expands the limits.

Fibre composites are widely used for space applications, such as solar arrays, antennas, optical platforms and supports for cryogenic tanks. One of the latest successfully launched satellites is the Infrared Space Observatory (ISO).

The lifetime of ISO is mainly limited due to the thermal conductivity of the cryogenic tank support structure.

Recent efforts show that optimized load adapted support structures can essentially decrease the thermal conductivity and thus increase the lifetime of such satellites.

The advantage of FRPs is the low specific weight at a relatively high stiffness and strength. [14] The main reason for using a lot of FRPs in the ISO structural parts is the low heat transmission from the outer support structure to the LHe tank inside, which should guarantee a long mission duration. A second effect is the reduction of additional thermal stresses in the structure when filling the tank.

Chapter 3

Normatives

3.1 ASTM

ASTM International - American Society for Testing and Materials - is a scientific and technical organization that develops and publishes voluntary standards on the characteristics of material, products, systems and services.

The standards includes test procedures for determining or verifying characteristics as chemical composition, measuring performance. The standards cover refined materials as steel and basic products as machinery and fabricated equipment.

3.1.1 D638 Plastics

The scope of ASTM-D638 test method covers the determination of the tensile properties of unreinforced and reinforced plastics in the form of standard dumbbell-shaped test specimens when tested under defined conditions of pretreatment, temperature, humidity, and testing machine speed.

[15] For Rigid and Semirigid Plastics the test specimen shall conform to the dimensions shown in Figs. 3.1 and 3.2.

The Type I specimen is the preferred specimen and shall be used where sufficient material having a thickness of 7 mm or less is available.

The Type II specimen is recommended when a material does not break in the narrow section with the preferred Type I specimen.

The Type V specimen shall be used where only limited material having a thickness of 4 mm or less is available for evaluation, or where a large number of specimens are to be exposed in a limited space.

The Type IV specimen is generally used when direct comparisons are required between materials in different rigidity cases (that is, nonrigid and semirigid).

The Type III specimen must be used for all materials with a thickness of greater than 7 mm but not more than 14 mm.

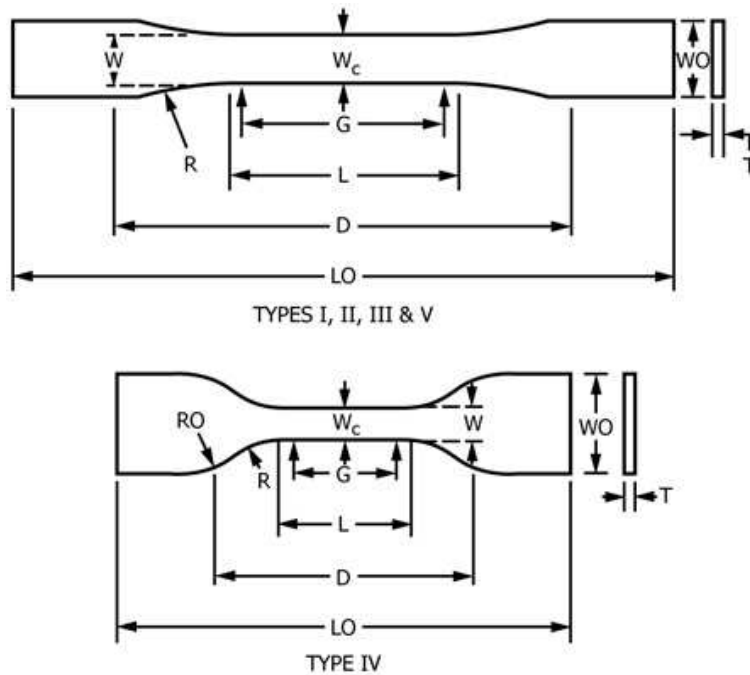


Figure 3.1. ASTM Specimen for Plastics.

Dimensions (see drawings)	7 (0.28) or under		Over 7 to 14 (0.28 to 0.55), incl	4 (0.16) or under	
	Type I	Type II	Type III	Type IV ^B	Type V ^{C,D}
<i>W</i> —Width of narrow section ^{E,F}	13 (0.50)	6 (0.25)	19 (0.75)	6 (0.25)	3.18 (0.125)
<i>L</i> —Length of narrow section	57 (2.25)	57 (2.25)	57 (2.25)	33 (1.30)	9.53 (0.375)
<i>WO</i> —Width overall, min ^G	19 (0.75)	19 (0.75)	29 (1.13)	19 (0.75)	...
<i>WO</i> —Width overall, min ^G	9.53 (0.375)
<i>LO</i> —Length overall, min ^H	165 (6.5)	183 (7.2)	246 (9.7)	115 (4.5)	63.5 (2.5)
<i>G</i> —Gage length ^I	50 (2.00)	50 (2.00)	50 (2.00)	...	7.62 (0.300)
<i>G</i> —Gage length ^I	25 (1.00)	...
<i>D</i> —Distance between grips	115 (4.5)	135 (5.3)	115 (4.5)	65 (2.5) ^J	25.4 (1.0)
<i>R</i> —Radius of fillet	76 (3.00)	76 (3.00)	76 (3.00)	14 (0.56)	12.7 (0.5)
<i>RO</i> —Outer radius (Type IV)	25 (1.00)	...

Figure 3.2. ASTM Specimen Dimensions for Plastics.

Number of Test Specimens has to be at least five specimens for each sample in the case of isotropic materials.

For anisotropic materials, when applicable, has to be five test specimens, normal to, and five parallel with, the principle axis of anisotropy.

The speed of testing has to be 5, 50 or 500 mm/min, with a nominal strain rate of 0.1, 1 or 10 mm/mm min respectively.

Engineering parameters to calculate are the Tensile Strength, the Elongation values, the Percent Elongation, the Percent Elongation at Yield, the Percent Elongation at

Break, the Nominal Strain, the Modulus of Elasticity, the Secant Modulus, the arithmetic mean of all values obtained and the "average value", and the standard deviation (estimated) with the equation in 3.1.

$$s = \sqrt{(\sum X^2 - n\bar{X}^2)/(n - 1)} \tag{3.1}$$

3.1.2 D3039 Reinforced Composites

The scope of ASTM-D3039 test method determines the in-plane tensile properties of polymer matrix composite materials reinforced by high-modulus fibers. [16] [17] [18] The composite material forms are limited to continuous fiber or discontinuous fiber-reinforced composites in which the laminate is balanced and symmetric with respect to the test direction.

Parameters To Be Specified Before Test are the tension specimen sampling method, coupon type and geometry (Fig. 3.3), the tensile properties and data reporting format desired, the environmental conditioning test parameters.

The Constant head-speed test has to have a standard head displacement rate of 2 mm/min.

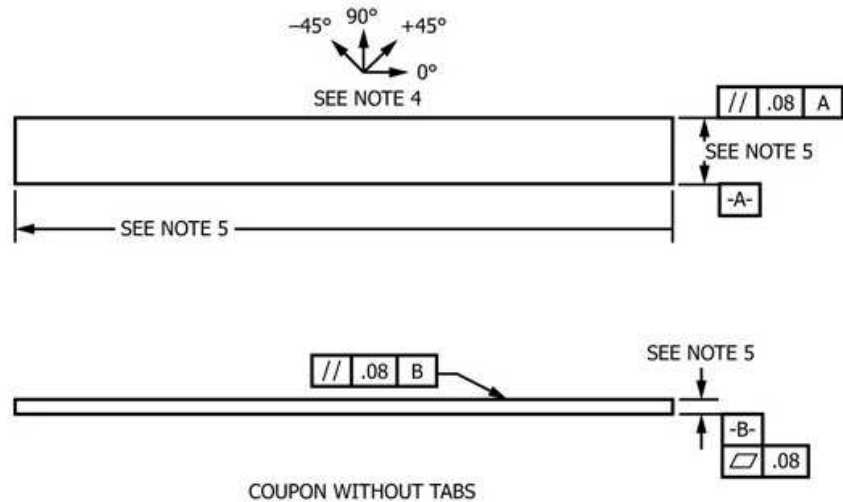


Figure 3.3. ASTM Specimen geometry for Composites.

Engineering parameters to calculate are the tensile strain, the tensile modulus of elasticity, the poisson's ratio, the standard deviation for each series of test. Select the specimen width and thickness to promote failure in the gage section and

assure that the specimen contains a sufficient number of fibers in the cross section to be statistically representative of the bulk material. The specimen length should normally be substantially longer than the minimum requirement to minimize bending stresses caused by minor grip eccentricities. Keep the gage section as far from the grips as reasonably possible and provide a significant amount of material under stress and therefore produce a more statistically significant result.

Fiber Orientation	Width, mm [in.]	Overall Length, mm [in.]	Thickness, mm [in.]	Tab Length, mm [in.]	Tab Thickness, mm [in.]	Tab Bevel Angle, °
0° unidirectional	15 [0.5]	250 [10.0]	1.0 [0.040]	56 [2.25]	1.5 [0.062]	7 or 90
90° unidirectional	25 [1.0]	175 [7.0]	2.0 [0.080]	25 [1.0]	1.5 [0.062]	90
balanced and symmetric random-discontinuous	25 [1.0]	250 [10.0]	2.5 [0.100]	emery cloth	—	—
	25 [1.0]	250 [10.0]	2.5 [0.100]	emery cloth	—	—

Figure 3.4. ASTM Specimen dimensions for Composites.

Recommendations on important dimensions are provided for typical material configurations in Fig. 3.4. These geometries have been found by a number of testing laboratories to produce acceptable failure modes on a wide variety of material systems, but use of them does not guarantee success for every existing or future material system.

To better understand the following sections, a brief description of the different used reference systems is given.

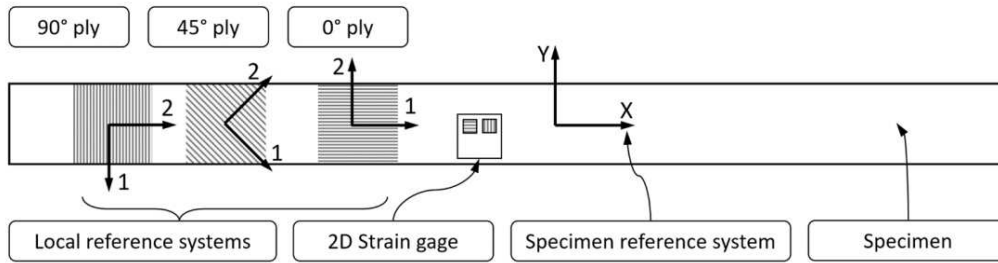


Figure 3.5. Reference picture, strain gage and specimen dimensions in scale.

- Referring to Fig. 3.5, two reference system are defined on each specimen:
- An X-Y-Z "specimen reference system" with a longitudinal X-axis and the Y-axis placed as to obtain a Z-axis exiting the bag-side of the panel from which the specimen has been cut;
 - A 1-2-3 "fiber reference system" with a 1-axis along fiber direction and the 2-axis

placed as to have a 3-axis coincident with the Z-axis.

Furthermore, on each fabricated panel, always rectangular shaped, has been defined another X-Y-Z "panel" reference system with a Z-axis defined as above, and an X-axis in the same direction of the longest edge of the plate (when defined).

3.1.3 D790 Flexural Properties of Unreinforced and Reinforced Plastics and Electrical Insulating Materials

These test methods cover the determination of flexural properties of unreinforced and reinforced plastics, including high-modulus composites and electrical insulating materials in the form of rectangular bars molded directly or cut from sheets, plates, or molded shapes. These test methods are generally applicable to both rigid and semirigid materials. These test methods utilize a three-point loading system applied to a simply supported beam.

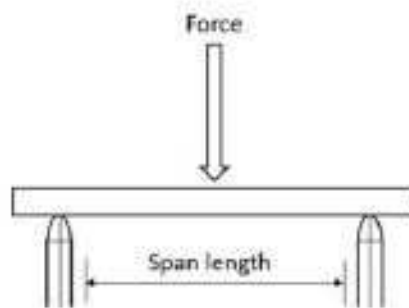


Figure 3.6. Three-point bending.

The three-point bending are performed following the ASTM standard D790. The flexural strength and stiffness are measured with test method where the specimen is loaded in the centre while resting on two supports as shown in Fig. 3.6.

According to the ASTM standard specimens, High-Strength Reinforced Composites that are less than 1.6 mm in thickness shall have a span length at least 16 times the specimen thickness. The length of the specimen is approximately 55 mm with 10% overlap on each end of the support span. The support span is 40 mm between the supports.

The rate of the crosshead was calculated by equations presented in ASTM standard D 790 and are dependent on the specimen dimensions as shown in equation 3.2.

$$R = \frac{ZL^2}{6d} [mm/min] \quad (3.2)$$

Where d is the depth of the beam, L is the support span, R is the crosshead motion and Z is the rate of straining.

The output from the testing machine are force and elongation. To find the flexural stiffness and maximum strength the data need to be converted to a stress-strain diagram.

The maximum stress at the outer surface at the midpoint between the supports.

The maximum strain is on the outer surface in the middle between the two supports.

The tangent modulus of elasticity, often called the "modulus of elasticity", is the ratio, within the elastic limit, of stress to corresponding strain.

It is calculated by drawing a tangent to the steepest initial straight-line portion of the load-deflection curve.

3.2 Applicability of current normatives to additive manufacturing of composites structures

The standards for tension tests utilize dog-bone or end tab specimens whose geometry is based on the thickness of the sample or the type of composite. Tension measurements provide Young's modulus, Poisson's ratio, Yield Stress, Strength, and Elongation to Break. The standards for composites address the orientation of fibers within a composite, but the applicability of such standards to AM materials has not been thoroughly described in the literature.

[19] ASTM D790 and ISO 178 are equivalent standards that utilize a three-point bend method to measure the flexural modulus, flexural strength, flexural stress and strain at break. These standards are applicable for unreinforced and reinforced materials.

ASTM and ISO standards were evaluated to determine their applicability to additive manufacturing. One of three classifications is given for each standard.

The list in Table 3.1 covers standards for plastic materials and composites. The following labels are used for assessing applicability of the standard:

- "Yes": the standard should be applicable for additive manufacturing with very minimal or no modifications.
- "Yes with guidance": the standard should be generally applicable for additive manufacturing, but there may be limits on its applicability, and some modifications or additional considerations are probably needed.
- "No": the standard requires specimens that cannot be built via AM, even major

modifications may not be adequate, another method is better suited for the measurement or the measurement simply is not applicable.

Standard designation	Standard name	Applicable for AM Testing
Tensile		
ISO 527-2	Plastics - Determination of tensile properties	Yes with guidance
ASTM D638-10	Standard Test method for tensile properties of plastics	Yes with guidance
ASTM D3039	Standard Test method for tensile properties of polymer matrix composite materials	Yes with guidance
ISO 527-4	Determination of tensile properties	Yes with guidance
ISO 527-5	Determination of tensile properties	No
Flexural		
ISO 178-10	Determination of stiffness in torsion of flexible materials	Yes with guidance
ASTM D6272-10	Standard test method for flexural properties of unreinforced and reinforced plastics and electrical insulating materials by four-point bending	Yes with guidance
ASTM D790-10	Standard test method for flexural properties of unreinforced and reinforced plastics and electrical insulating materials	Yes with guidance
Shear		
ASTM D3518-13	Standard test method for Inplane shear response of polymer matrix composite materials by tensile test of +-45deg	No
ASTM 2344-13	Standard test method for short-beam strength of polymer matrix composite materials and their laminates	No
ISO 15310-99	Fibre reinforced plastic composites - Determination of the inplane shear modulus by the plate twist method	Yes with guidance

Table 3.1. Standards Applicability Assessment.

3.3 State of art - Current literature

In "Characterization of mechanical properties and fracture mode of additively manufactured carbon fiber and glass fiber reinforced thermoplastics" [30], the fused filament fabrication technique is employed to fabricate continuous carbon and glass FRTP composites and its microstructural characteristics and the resulting tensile, flexural, and quasi-static indentation characteristics of the printed composites are examined. Additionally, the fracture behavior of each test sample is evaluated and discussed in detail.

In "Evaluation and prediction of the tensile properties of continuous fiber-reinforced 3D printed structures" [29] commercial desktop 3D printers have become available which produce functional 3D printed parts.

The aim of this study is to evaluate the elastic properties of the fiber reinforced 3D printed structures and predict elastic properties using an Average Stiffness (VAS) method. Samples evaluated in this study were produced by varying the volume fraction of fibers within the 3D printed structures. The model presented will allow for designers to predict the elastic properties of fiber reinforced 3D printed parts to be used for functional components which require specific mechanical properties.

In "Investigation of microstructure and mechanical properties of 3D printed Nylon" [31] a multiscale investigation and characterization of additive manufactured Polyamide material using fused deposition modelling technique is presented.

A multiscale investigation dedicated to minimizing the effect of shape distortion during 3D printing are presented, focusing on both molecular alignment in microstructure and implementing internal structures in mesostructure. Characterization on samples investigating microstructure was performed with coefficient of linear thermal expansion measurement and 3-point bending experiment.

Different samples with varying infill patterns are tested and results indicates an isotropic behaviour through the manufactured samples and implies no molecular alignment due to printing pattern.

In meso-structure, an implemented internal pattern is investigated. All samples are measured with 3D scanning equipment to localize and measure the magnitude of shape distortion. Attempts to find relationships in shape distortion and porosity between the samples resulted in no observed trends. Compressive experiments were performed on samples in axial and transverse directions resulting in anisotropic behaviour.

Chapter 4

Preparation for testing

4.1 Markforged 3D Printing

The 3D printer used in this report is a Markforged Mark Two 3D printer. The printer type is Fused deposition modelling (FDM) and Composite filament fabrication (CFF) which means that it can print with both thermoplastic material and continuous fibres such as Kevlarcarbon and fibreglass. The printer has two extruder heads, one to plastic material and one to fibre material. This enables mixing the fibres and plastic material in the structure to improve the mechanical properties. The dimensions of the 3D printer are 575x322x360 millimetres with a minimum height of 100 microns. The Markforged Mark one printer is shown in fig 4.1.

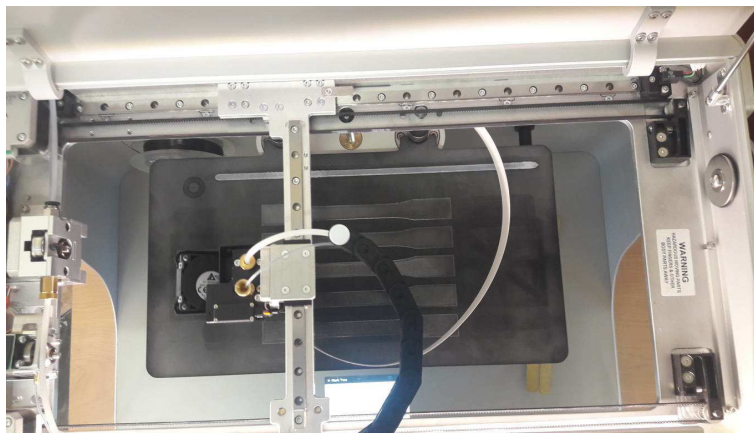


Figure 4.1. Markforged - Mark Two 3D printer.

The Markforged Mark Two 3D printer is not open source and limited to the 3D printing software Eiger. Eiger is Markforgeds own 3D-printing software and have

limitations of changing several printing parameters. The printing parameters that can be changed are structural parameters such as infill pattern, infill densities, layer height, amount of wall, roof and bottom layers. The nozzle temperature used to extrude the nylon material have a temperature of 266 degrees. Before starting to print the samples, some 3D printer configurations are done to obtain the best results. The printer bed is first levelled to the correct distance from the extruder. The bed is later slightly heated with water to clean the surface. Before mounting the bed in the printer, a glue is placed on the area where the part will be printed on the bed. The glue will increase the adhesion between the bed and material to avoid warping and that the part finally dislocate.

[20] [21] The materials used in this project are Nylon (Polyamide) and Carbon fiber provided by Markforged. The materials are by the manufacturer suitable specific for the Markforged 3D printer and the provided material data is presented in table 4.1.

Parameters	Nylon	Carbon Fiber	Kevlar
Tensile Strenght (MPa)		700	610
Tensile Modulus (GPa)	0.94	54	27
Tensile strain at break (%)	260	1.5	2.7
Flexural Strength (MPa)	32	470	190
Flexural Modulus (GPa)	0.84	51	26
Density (g/cm ³)	1.1	1.4	1.2

Table 4.1. Markforged parameters.

Markforged’s printing software Eiger have some built in infill patterns such as rectangular, hexagonal and triangular pattern. The work in this project is regarding to all the available patterns. With the rectangular pattern, it was possible to print in a 0 deg, 90 deg and minus 45 deg, plus 45 deg layup as illustrated in Figure 4.2.

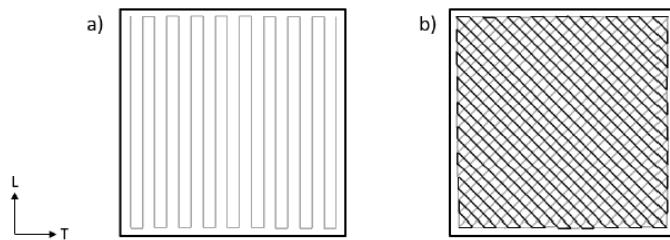


Figure 4.2. Unidirectional and $+45^\circ$ rectangular infill pattern.

Another infill pattern that is analysed in this project is triangular pattern as shown in Figure 4.3. This is an infill pattern that increase speed while still making a strong part. Recommendations from Markforged states that the infill percentage should be below 80% to avoid warping of the printed parts.

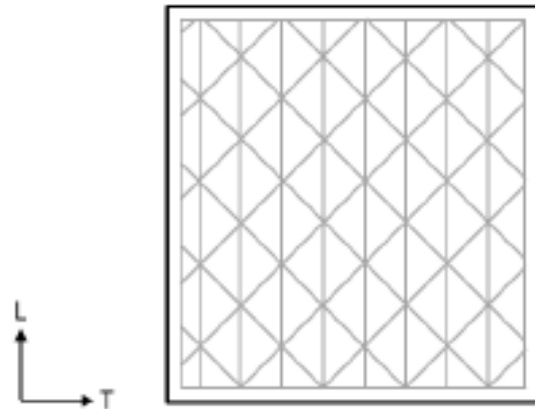


Figure 4.3. Triangular infill pattern.

Fig. 4.4 shows the final setup before printing of 5 composite samples in order to optimize the printing time shown on the top left. It is shown also the volume of each material and the total cost of the printing.

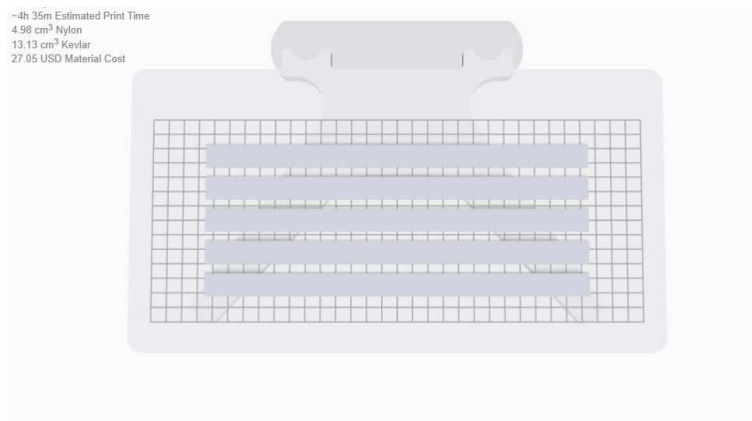


Figure 4.4. Setup before printing.

4.2 Samples Manufacturing

In Table 4.2 are listed all sample codes used to recognize and differentiate the printed and subsequently tested batches of specimens.

Nylon	Carbon Fiber
N02R100F10	NC0125F2W1D0
N02R50F4	NC0125F3W2D0
N02H50F4	NC0125F4W1D90
N02T25F4	NC0125F1W1D0
N02T50F4	NC0125L50p8F1W1D0
N02T75F4	NC0125L90p16F1W1D0

Table 4.2. Sample codes.

The first letter indicates the material used: 'N' for Nylon material or 'NC' for Nylon and Composite material.

The first numbers indicate the layer height: '02' for 0.2 mm nylon specimens and '0125' for 0.125 mm carbon fiber specimens.

For nylon samples 'R', 'T', and 'H' indicate rectangular, triangular, and hexagonal pattern of material respectively. Subsequently '100' or '50' indicate the density of the material.

Meanwhile 'L' with a number ahead indicates the span length, 'p' is the number of layers, 'F' with a number ahead indicates the number of floor layers, 'W' the number of wall layers, and D the fiber angles.

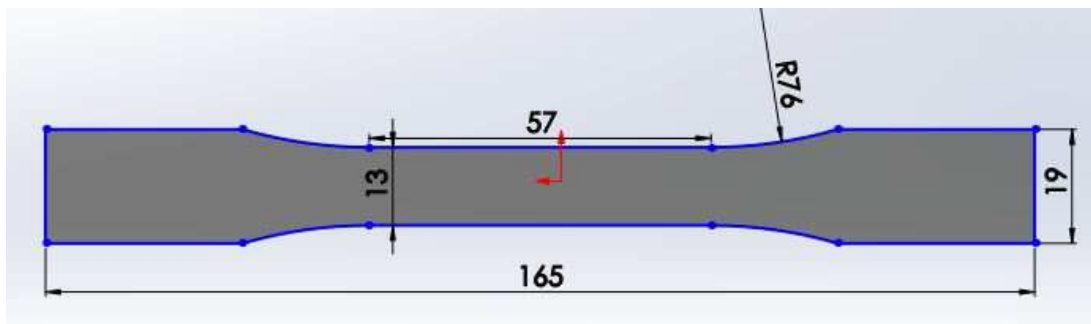


Figure 4.5. Nylon sample CAD.

Nylon samples as expressed in ASTM D638-14 'Standard Test Method for Tensile Properties of Plastics' have a length of 165 mm, a width of 19 mm and a thickness

of 3.2 mm. It is been used Nylon sample CAD as shown in Fig. 4.5.

Instead 0° carbon fiber angles samples and 90° carbon fiber angles samples have 2 different geometries.

The first ones are longer but with less width measuring exactly 250x15x1 mm, while the second ones measure 175x25x2 mm. Carbon fiber sample CAD for traction test is shown in Fig. 4.6.

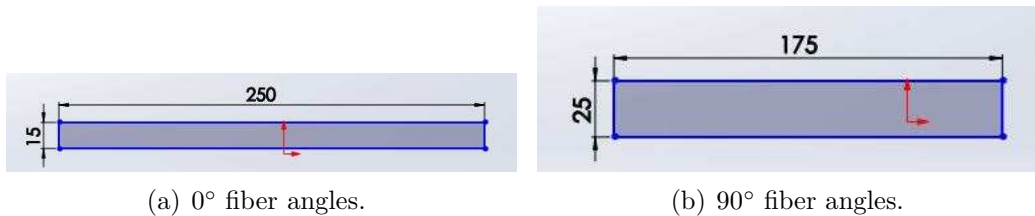


Figure 4.6. Carbon fiber sample CAD for traction test.

4.2.1 Nylon specimens

A plan view of nylon specimens is reported in Fig 4.7.

How we can note all specimens have been painted with white paint in order to be subsequently painted with black irregular points for digital image correlation.

[22] A following chapter is dedicated to this part of study.

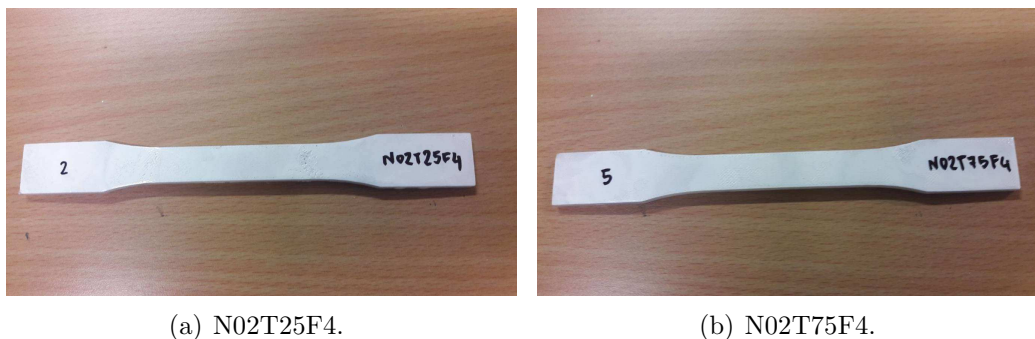


Figure 4.7. Nylon samples.

All nylon batches specimens with different patterns are listed below. 2 types have rectangular pattern, 3 triangular pattern, and only 1 hexagonal pattern. So there are 6 different batches of specimens studied. For each type it has been printed 5 specimens, except to 'N02R100F10' because it has been printed 6, and 'N02R50F4' because it has been printed 7.

It has been used 0.2 mm height for each layer, 100% density for only 'N02R100F10' sample and 50% density for all other specimens.

The number of floor layers have been the same for all nylon specimens (4), except to 'N02R100F10' batches of samples (10).

A software internal view of hexagonal and triangular pattern is shown in Fig. 4.8 and 4.9.

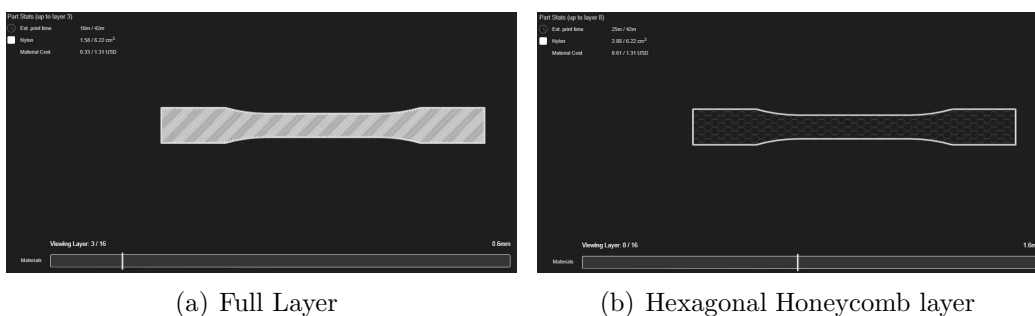


Figure 4.8. Software internal view of a hexagonal pattern.

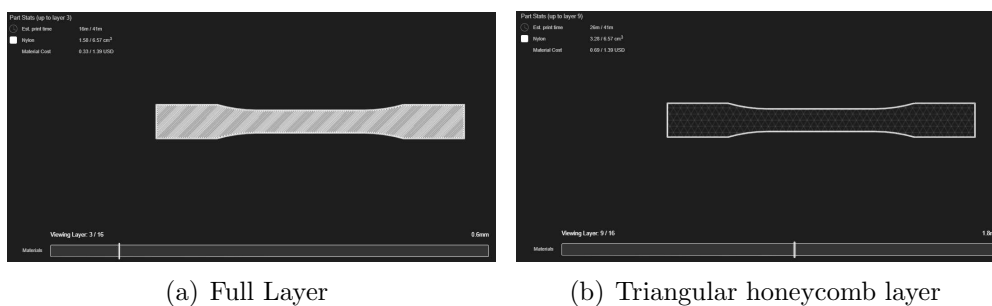


Figure 4.9. Software internal view of a triangular pattern.

4.2.2 Carbon Fiber specimens

All carbon fiber batches specimens are now listed.

The main difference between the batches of carbon fiber samples is in the study of different floor, wall layers, and fibre angles. The geometry and the material composition of the layers are also not equal. In fact the below and the upper layer are made by nylon, while the middle layer by carbon fiber.

[23] [24] [25] A plan view of carbon fiber specimens is reported in Fig 4.10.

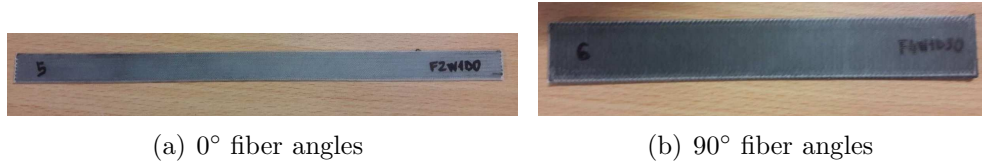


Figure 4.10. Carbon Fiber samples.

There are 3 different batches of specimens studied for traction test. For each type it has been printed 7 specimens, except to 'NC0125F4W1D90' that has been printed 6.

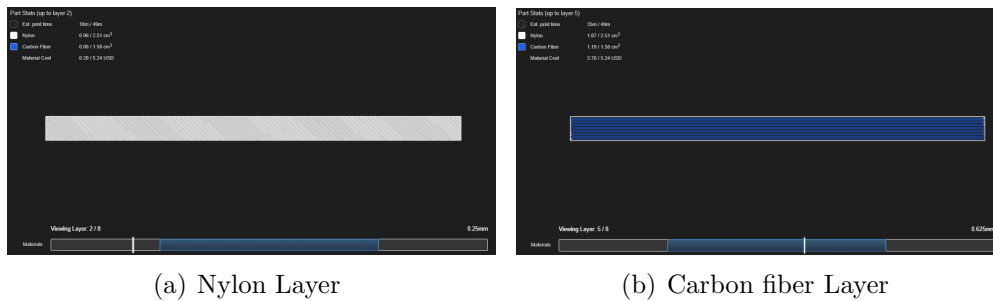
It has been used 0.125 mm height for each layer, 50% density for all the specimens. The number of floor layers are 2, 3 and 4, while the number of wall layers are 1 or 2, and fiber angles are 0° and 90°.

The main differences of part setting for each batch of specimens is shown in Table 4.3.

Part Settings	NC0125F2W1D0	NC0125F3W2D0	NC0125F4W1D90
Layer Height (mm)	0.125	0.125	0.125
Fill pattern	Triangular	Triangular	Triangular
Fill density	50%	50%	50%
Floor Layers	2	3	4
Wall Layers	1	2	1
Total Layers	8	8	16
Fiber Angles	0	0	90

Table 4.3. Carbon fiber samples part settings for traction test.

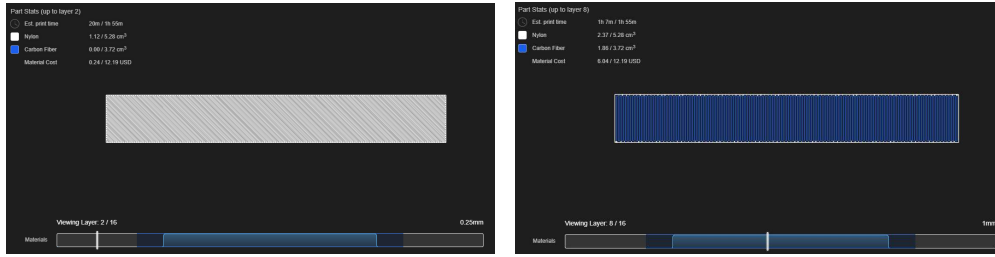
A software internal view for different angle fiber batch of specimens is shown in Fig. 4.11, 4.12.



(a) Nylon Layer

(b) Carbon fiber Layer

Figure 4.11. NC0125F2W1D0 Software internal view.



(a) Nylon Layer

(b) Carbon fiber Layer

Figure 4.12. NC0125F4W1D90 Software internal view.

There are 2 different batches of specimens studied for three-point bending test: "NC0125L50p8F1W1D0" and "NC0125L90p16F1W1D0". It has been used 0.125 mm height for each layer, and 100% density for all the specimens.

The main differences of part setting for each batch of specimens is shown in Table 4.4.

Part Settings	NC0125L50p8F1W1D0	NC0125L90p16F1W1D0
Layer Height (mm)	0.125	0.125
Fill pattern	Rectangular	Rectangular
Fill density	100%	100%
Floor Layers	1	1
Wall Layers	1	1
Total Layers	8	16
Fiber Angles	0	0
Span length	50	90

Table 4.4. Carbon fiber samples part settings for 3pb.

4 carbon fiber specimens have been printed for three-point bending tests, following D790-ASTM norms.

3 samples with 50 mm of length span and 1 sample with 90 mm of length span have been printed.

Fig. 4.13 shows a plan view of each sample.

ASTM D790 suggests that the span length should be about 40 times longer than total thickness.



Figure 4.13. 0 ° carbon fiber specimens for 3pb test.

4.2.3 Carbon Fiber plates

All carbon fiber plates are now listed.

It is shown in Fig. 4.14 0° carbon fiber plate with its code NC0125F1W1D0.

The material composition of the layers is equal to the carbon fiber samples but the number of the layers changes.

It has been obtained 5 specimens through the water jet cutter.



Figure 4.14. 0 ° carbon fiber plate.

It has been used 0.125 mm height for each layer, 100% nylon density for all the plates. The number of floor layers and the number of wall layers are 1 for each one. NC0125F1W1D0 plate is made by 8 carbon fiber internal layers, 1 upper and 1 lower nylon layers.

It is shown in Fig. 4.15 the machine used to cut the plate. A water jet cutter, also known as a water jet or waterjet, is an industrial tool capable of cutting a wide variety of materials using a very high-pressure jet of water, or a



Figure 4.15. Water jet cutter.

mixture of water and an abrasive substance.

Waterjet cutting is an economical way to cut 2D shapes in a very wide range of materials with no tooling costs. The unique process provides reasonably good edge quality, no burrs and usually eliminates the need for secondary finishing processes. Waterjets also generate no heat so the material edge is unaffected and there is no distortion.

4.3 Dimensional accuracy

Measurements for A, B, and C section have been taken for each lot.

In this section it has been presented the average widths, thicknesses and areas of the "B" central part of the sample shown in Fig. 4.16.



Figure 4.16. Plan view of the sample section.

4.3.1 Nylon

For the middle section of each sample it is shown in Table 4.5 the width and the thickness averages for each nylon batch of specimens, with the respective standard deviation in millimeters.

For each batch of nylon specimens it is shown in Fig. 4.17 the average areas of each sample.

Nylon	Width	St. Deviation	Thickness	St. Deviation
N02R100F10	13.26	0.0956	3.68	0.1039
N02R50F4	13.13	0.1037	3.56	0.0871
N02H50F4	13.05	0.0911	3.49	0.0619
N02T25F4	13.03	0.0335	3.45	0.0702
N02T50F4	13.06	0.0508	3.55	0.0365
N02T75F4	13.14	0.0709	3.51	0.0550

Table 4.5. Nylon Width and Thickness Averages.

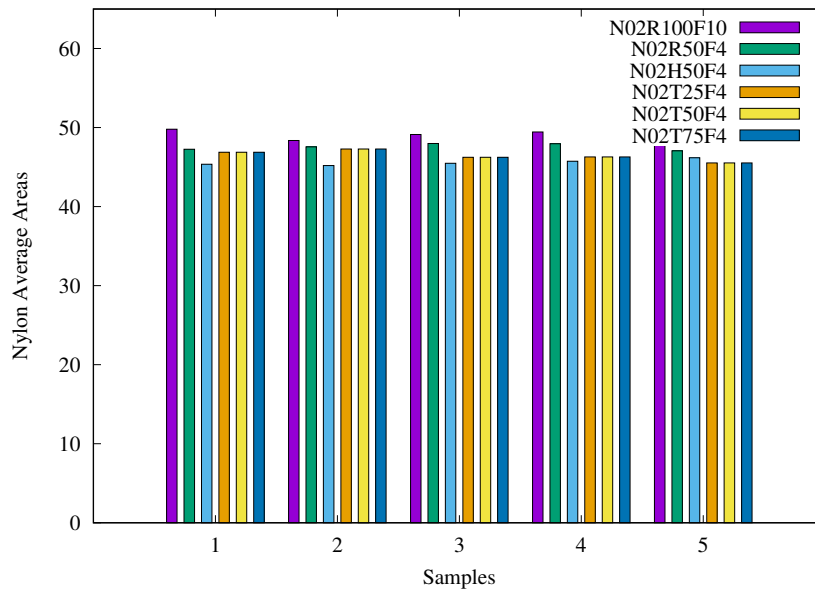


Figure 4.17. Average Areas for each batch of Nylon samples.

4.3.2 Carbon Fiber

For the middle section it is shown in Table 4.6 the width and the thickness averages for each carbon fiber batch of specimens, with the respective standard deviation in millimeters.

For each batch of Carbon fiber specimens it is shown in Fig. 4.18 the average areas of each sample.

The nominal dimensions of NC0125F1W1D0 plate are 270x90x1.25 mm³. It has been obtained 5 250x15x1.25 mm³ samples.

Carbon Fiber	Width	St. Deviation	Thickness	St. Deviation
NC0125F2W1D0	15.05	0.0623	1.26	0.0967
NC0125F3W2D0	15.15	0.0787	1.21	0.0718
NC0125F4W1D90	25.06	0.0366	2.22	0.0606
NC0125F1W1D0	15.29	1.5191	1.58	0.2139
NC0125L50p8F1W1D0	13.0	0.0	1.47	0.0577
NC0125L90p16F1W1D0	13.1	0.0	2.42	0.0

Table 4.6. Carbon Fiber Width and Thickness Averages.

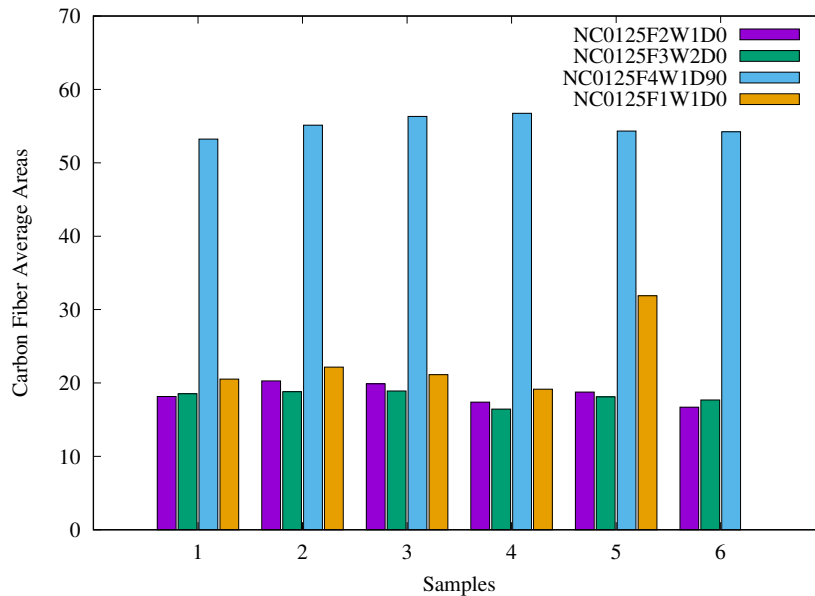


Figure 4.18. Average Areas for each batch of Carbon fiber samples.

NOTE: It's important to notice that only one nylon layer of NC0125F1W1D0

lot is remained attached to the plate after printing. The layers composition of each NC0125F1W1D0 sample after water jet cutting is shown in Table 4.7.

Sample	Nylon layers	Carbon Fiber layers
1	2	8
2	1	8
3	1	7
4	1	7
5	1	8

Table 4.7. NC0125F1W1D0 layers composition.

Figure 4.19 shows the average areas for each batch of three-point bending carbon fiber samples.

The nominal area for the firsts 3 samples measures 16.25 mm², while the nominal area for the fourth sample measures 29.25 mm².

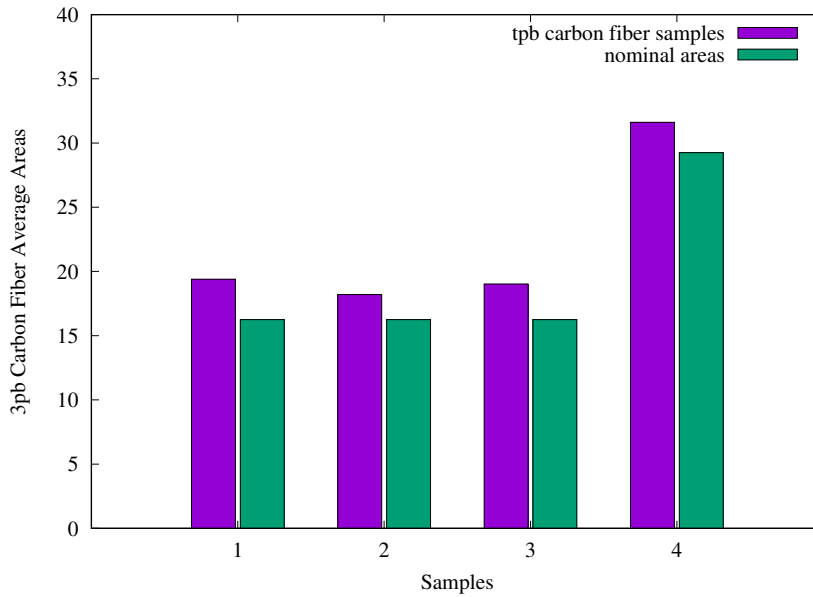


Figure 4.19. Average Areas for each batch of 3pb Carbon fiber samples.

4.3.3 Comparison between Dimensions Norms - Reality

Nylon samples as expressed in ASTM D638-14 'Standard Test Method for Tensile Properties of Plastics' must have 13 mm of width and 3.2 of thickness.

Table 4.8 shows the percentage of volume of nylon samples provided by Eiger software.

Sample	% Honeycomb Volume	% Nylon Volume
N02R100F10	% 0.0	% 100.0
N02R50F4	% 45.6	% 54.5
N02H50F4	% 45.6	% 54.5
N02T25F4	% 45.6	% 54.5
N02T50F4	% 45.6	% 54.5
N02T75F4	% 45.6	% 54.5

Table 4.8. Volume Percentage of Nylon Samples.

Carbon fiber samples as expressed in ASTM D3039/D3039M 'Standard Test Method for Tensile Properties of Polymer Matrix Composite Materials' must have 15 or 25 mm of width and 1 or 2 mm of thickness, depending on the geometry of the sample.

For NC0125F1W1D0 lot the thickness has been improved to 1.25 mm in order to optimize the traction test on the carbon fiber.

Table 4.9 shows the percentage of volume of carbon fiber samples provided by Eiger software.

Sample	% Carbon Fiber Volume	% Nylon Volume
NC0125F2W1D0	% 38.6	% 61.4
NC0125F3W2D0	% 16.0	% 84.0
NC0125F4W1D90	% 41.3	% 58.7
NC0125F1W1D0	% 75.5	% 24.5
NC0125L50p8F1W1D0	% 65.8	% 34.2
NC0125L90p16F1W1D0	% 76.4	% 23.6

Table 4.9. Volume Percentage of Carbon fiber Samples.

4.4 Microscopic measurements

Microscopic section measurements have been taken by Leica z16 APO-A microscope shown in Fig. 4.20.

Fig. 4.21 shows the width of attached Carbon Fibers. It can see a width of 2.288 mm in the straight view, while 2.134 mm in the curvilinear profile.

Fig. 4.22 shows 2 carbon fiber sections. The first one has been crushed and its experimental measurements have been taken.

The diameter of the oval profile is 0.306 mm measuring the shortest length and 0.496 mm measuring the longest length.

The second one's diameter measures 0.378 mm.

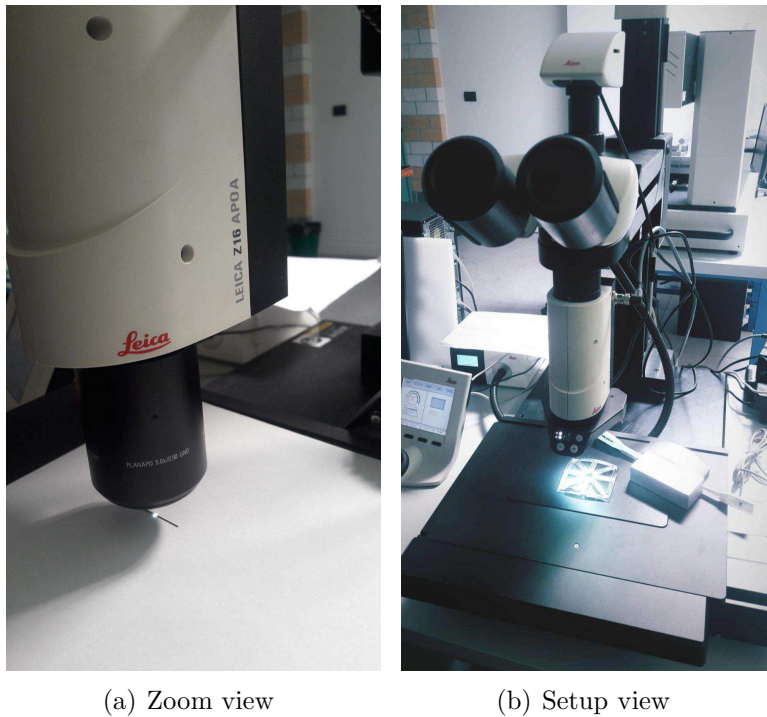


Figure 4.20. Microscope lens.

Fig. 4.23 shows a single fiber width that measures 0.364 mm.

Fig. 4.24 shows 2 carbon fiber details. The first one photo shows a crack of about 400 microns.

The second detail shows the distance between the single fibers and the average measure is of about 8 microns.

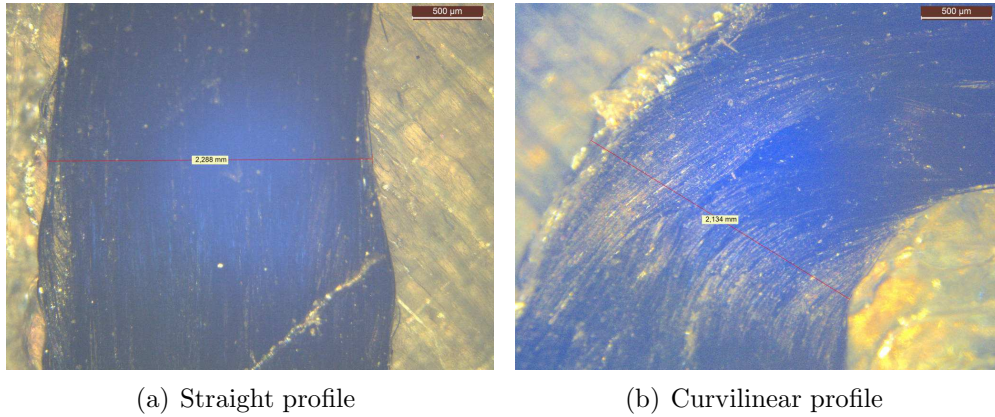


Figure 4.21. Width of attached Carbon Fibers.

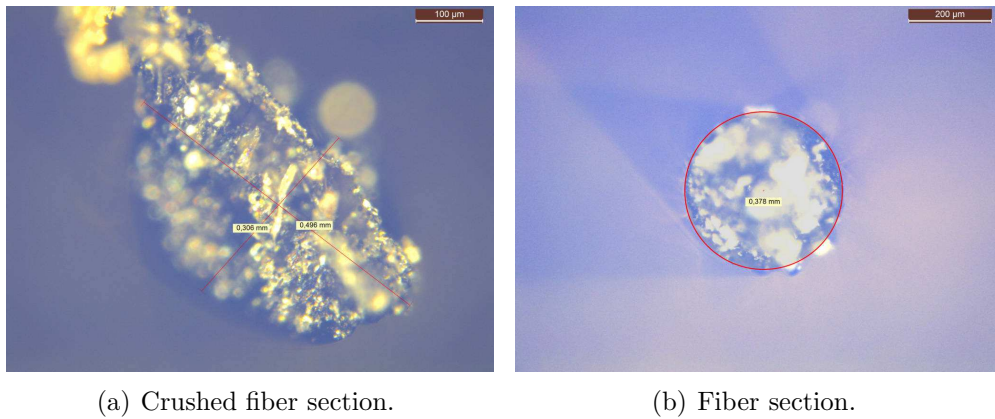


Figure 4.22. Fiber sections.

Fig. 4.25 shows how composite fracture follow the internal pattern chosen. It is visible in the first photo the distance between 2 layers measuring about 0.338 mm. In this case 2 external layers have been printed. The second photo shows a plan view of the composite break in one of the printed samples.

Fig. 4.26 and the first photo of Fig. 4.24 show the thickness measuring 0.125 mm of each single layer.

The second photo of Fig. 4.27 shows the second sample of N02R100F10 lot. It has been measured after crushing and its dimensions are heterogeneous and lower than nominal measurements. It is visible also the white paint used to digital image correlation.

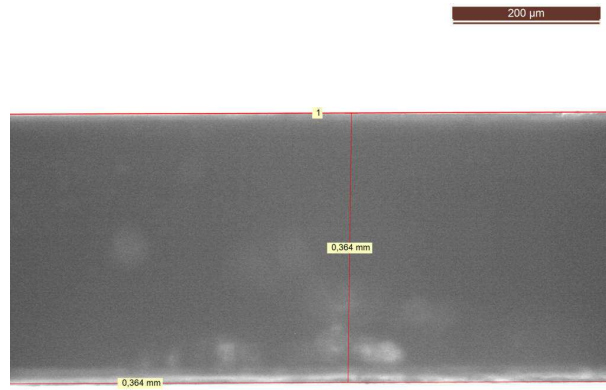
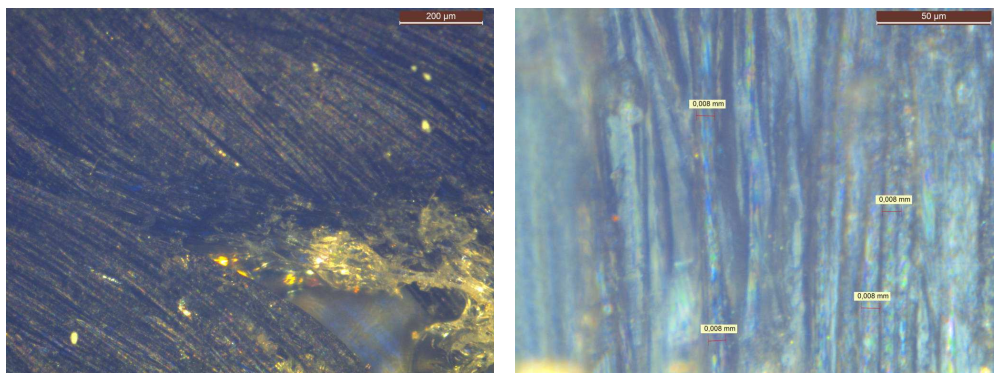


Figure 4.23. Single Fiber width.



(a) Crushed fiber detail.

(b) Single fibers detail.

Figure 4.24. Fibers detail.

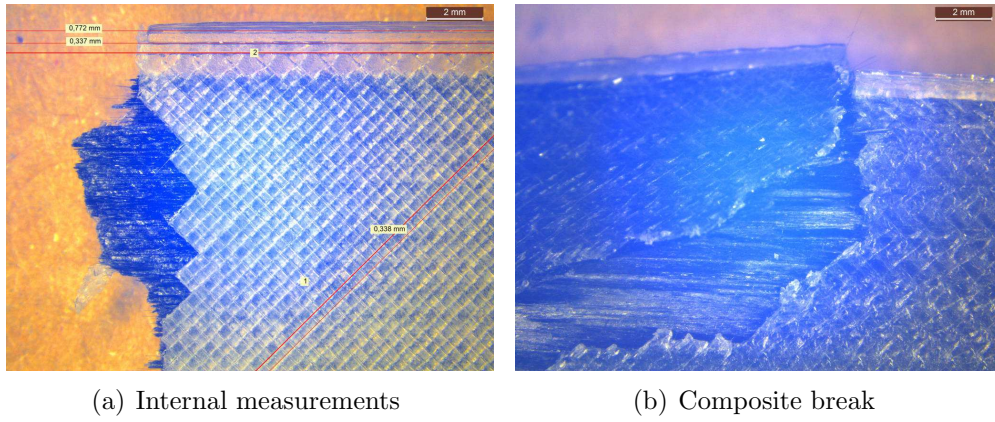


Figure 4.25. Composite Fracture.

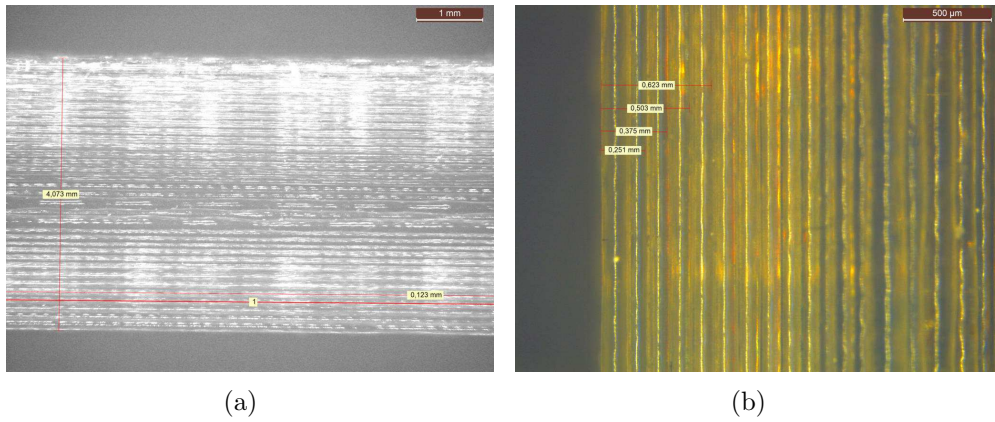


Figure 4.26. Lamination.

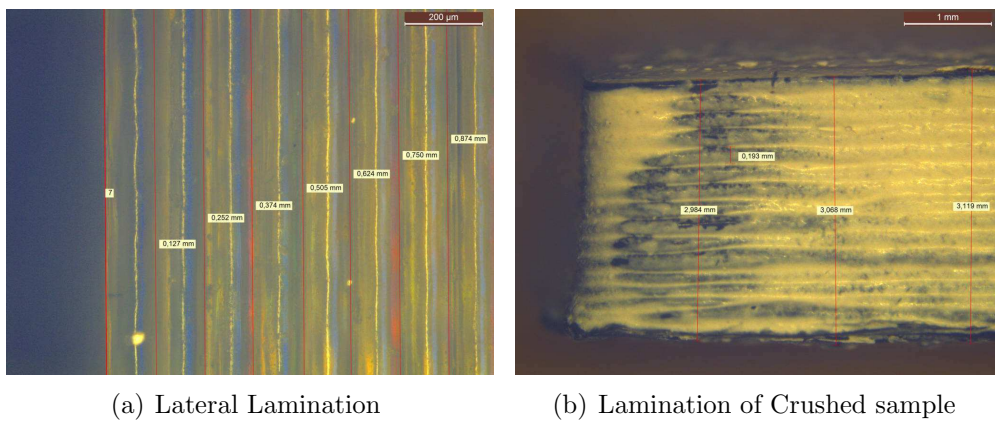


Figure 4.27. Lateral view lamination.

Chapter 5

Traction test



Figure 5.1. Traction test setup.

Traction test has been proceed in order to solicit each sample until break. Fig. 5.1 shows the traction test setup.

ASTM normatives has been respected in order to measure displacements for each strain developed on the samples.

Different velocities has been used to take measurements as multiple as possible in order to compare final results.

It is important to point out that not all the samples subjected to stress have been broken for different reasons analyzed in the following paragraphs.

Fig. 5.2 shows NC0125F1W1D0 specimen after traction test. It is visible how almost all the fibers came out of their longitudinal axis.



Figure 5.2. Carbon fiber specimen after traction test.

5.1 Sigma-epsilon graphs

Sigma-epsilon graphs are useful to understand the breaking test behaviour. Loads and displacements has been given from the software after the break.

Dividing the loads to the involved area and the displacements to the gage length, sigma-epsilon graphs have been obtained through a simple iteration for each step studied from the software.

5.1.1 Nylon and Carbon fiber compared between Standard velocities

Figure 5.3 shows that 2, 3, 4, and 5 sample of Rectangular Nylon N02R100F10 have been analyzed.

Standard velocity has been 50 mm/min.

It is possible to recognize a similar behaviour for each sample in the linear part and in the non linear curve.

In the first graph the curve arrives to 1500 N until breaking, while in the second graph it reaches about 30 MPa.

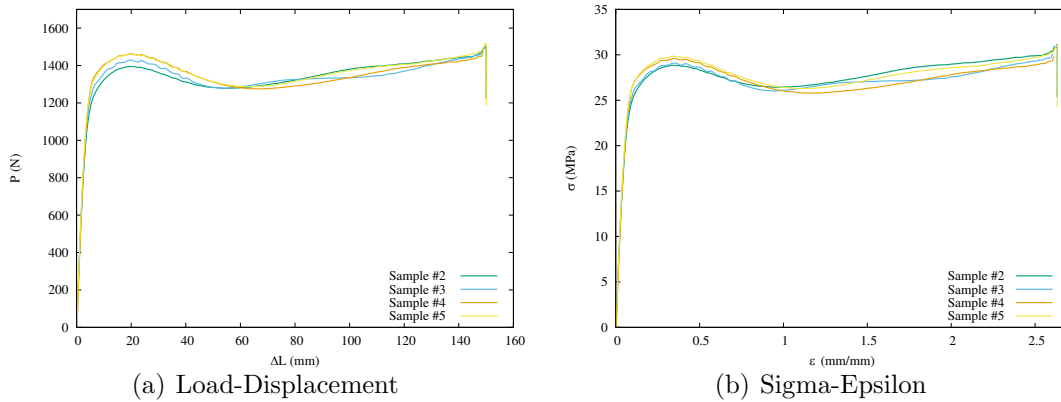


Figure 5.3. Rectangular Nylon N02R100F10.

Figure 5.4 shows that 3, 4, and 5 sample of Rectangular Nylon N02R50F4 have been analyzed.

Standard velocity has been 50 mm/min.

It is possible to recognize a similar behaviour for each sample in the linear part until 15 MPa, while in the non linear curve the fifth sample has been solicited at a higher load than 2 others, so this effect it is visible also to the second graph.

In the first graph the curve arrives to 1200 N until breaking, while in the second graph it reaches about 25 MPa.

Figure 5.5 shows that 2 and 3 sample of Hexagonal Nylon N02H50F4 have been analyzed.

Standard velocity has been 50 mm/min.

It is possible to recognize a similar behaviour for each sample in the linear part until 15 MPa, while in the non linear curve the third sample has higher displacements although it has been solicited at the same load of the second sample, so this effect it is visible also to the second graph.

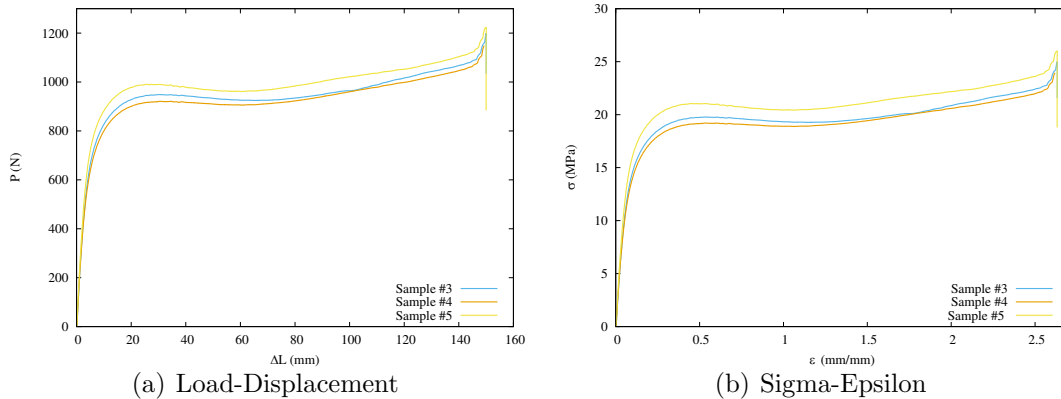


Figure 5.4. Rectangular Nylon N02R50F4.

In the first graph the curve arrives to 850 N until breaking, while in the second graph it reaches about 17 MPa.

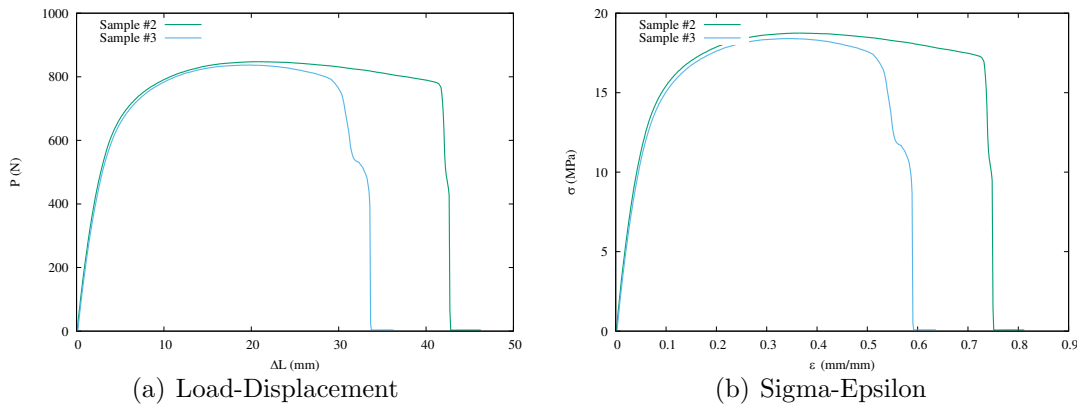


Figure 5.5. Hexagonal Nylon N02H50F4.

Figure 5.6 shows that 1, 2, 3, 4 and 5 sample of Triangular Nylon N02T25F4 have been analyzed.

Standard velocity has been 50 mm/min.

It is possible to recognize a similar behaviour for each sample in the linear part until 15 MPa, while in the non linear curve the first and the fourth sample have higher displacements although it has been solicited more or less than the same load of the other samples, so this effect it is visible also to the second graph.

In the first graph the curve arrives about to 900 N until breaking, while in the second graph it reaches about 20 MPa.

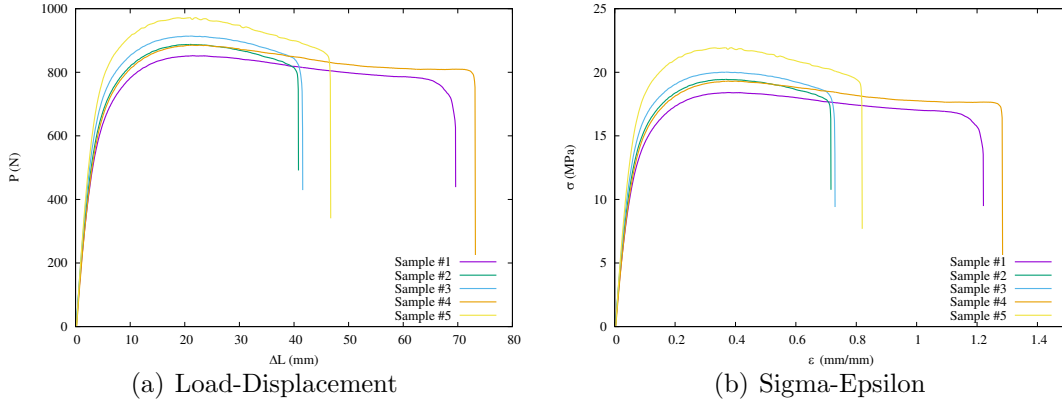


Figure 5.6. Triangular Nylon N02T25F4.

Figure 5.7 shows that 1, 2, 3, 4 and 5 sample of Triangular Nylon N02T50F4 have been analyzed.

Standard velocity has been 50 mm/min.

It is possible to recognize a similar behaviour for each sample in the linear part until 12 MPa, while in the non linear curve the fifth and the fourth sample have lower displacements and it has been solicited more than the same load of the other samples, so this effect it is visible also to the second graph.

In the first graph the curve arrives about to 800 N until breaking, while in the second graph it reaches about 15 MPa.

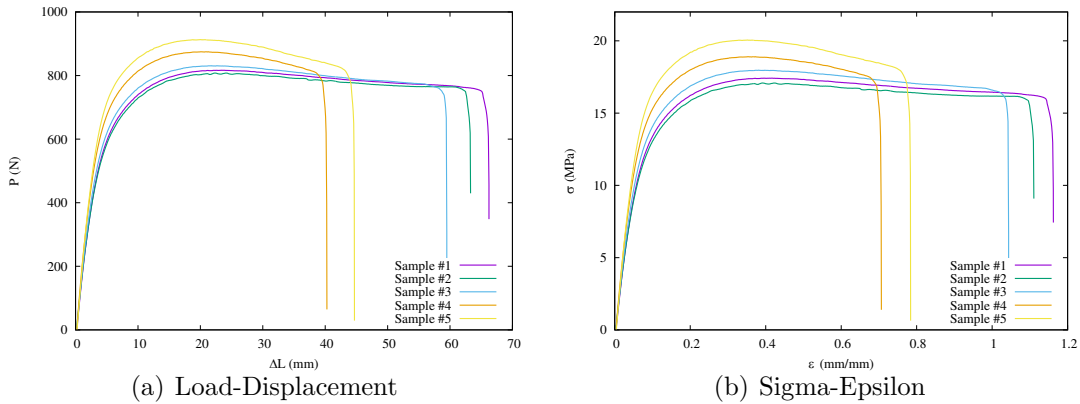


Figure 5.7. Triangular Nylon N02T50F4.

Figure 5.8 shows that 1, 2, 3, 4 and 5 sample of Triangular Nylon N02T75F4 have been analyzed.

Standard velocity has been 50 mm/min.

It is possible to recognize a similar behaviour for each sample in the linear part and in the non linear curve.

In the first graph the curve arrives about to 1000 N until breaking, while in the second graph it reaches about 22 MPa.

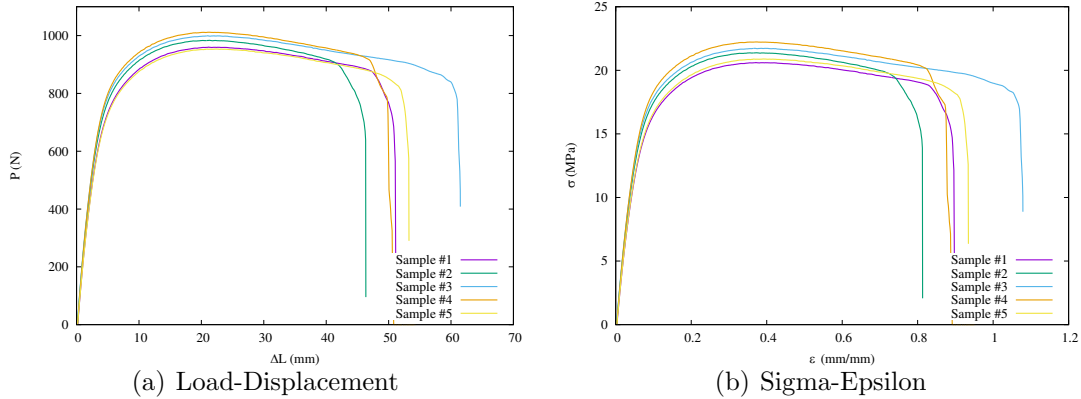


Figure 5.8. Triangular Nylon N02T75F4.

Figure 5.9 shows that 1, 2, 3, 4, 5, 6 and 7 sample of Carbon fiber NC0125F2W1D0 have been analyzed.

Standard velocity has been 2 mm/min.

It is possible to recognize in the first graph a similar behaviour for each sample.

The second graph shows different curves caused to the different areas of each sample.

In the first graph the straight line arrives about to 6500 N until breaking, while in the second graph it reaches about 350 MPa.

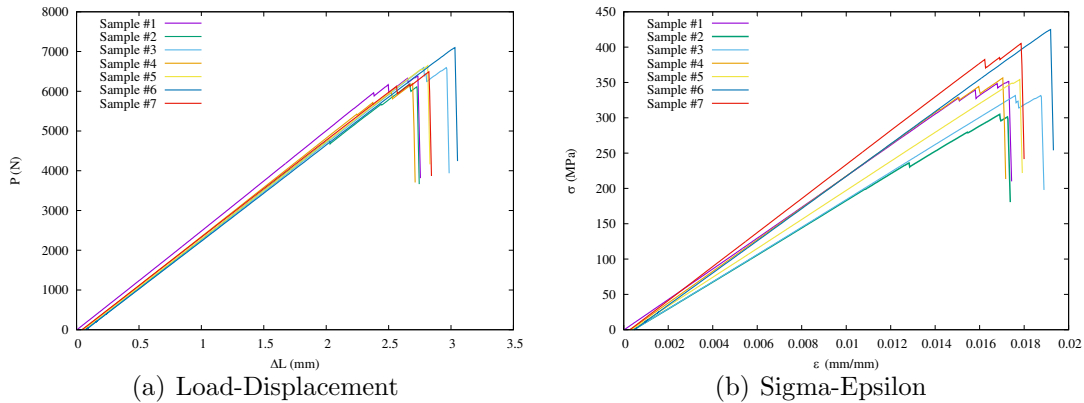


Figure 5.9. Carbon fiber NC0125F2W1D0.

Figure 5.10 shows that 1, 2, 3, 4, 5, 6 and 7 sample of Carbon fiber NC0125F3W2D0 have been analyzed.

Standard velocity has been 2 mm/min.

It is possible to recognize in the first graph a similar behaviour for each sample.

The second graph shows different curves caused to the different areas of each sample.

In the first graph the straight line arrives about to 3000 N until breaking, while in the second graph it reaches about 150 MPa.

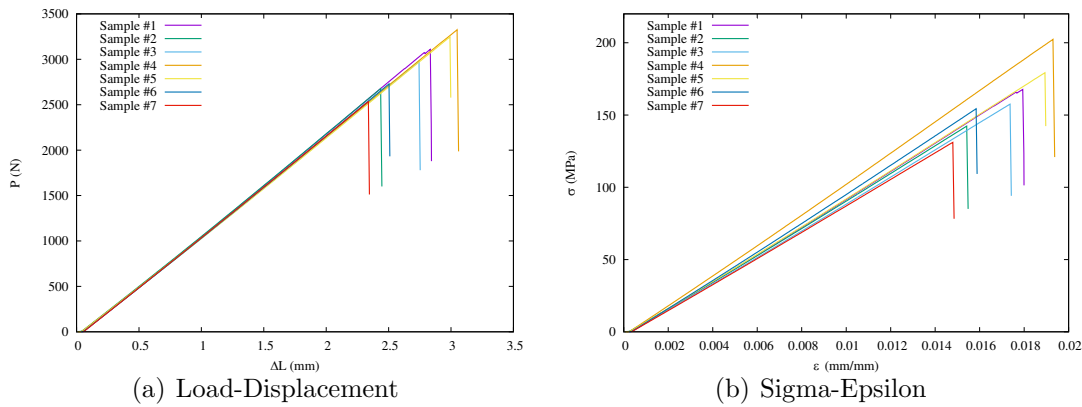


Figure 5.10. Carbon fiber NC0125F3W2D0.

Figure 5.11 shows that 1, 2, 3, 4, 5, and 6 sample of Carbon fiber NC0125F4W1D90 have been analyzed.

Standard velocity has been 2 mm/min.

It is possible to recognize a similar behaviour for each sample in the linear part.

The non linear curves are progressively descendent caused to the lack of the breaking point.

In the first graph the straight line arrives about to 900 N until breaking, while in the second graph it reaches about 15 MPa.

Figure 5.12 shows that 1, 2, 3, 4, and 5 sample of Carbon fiber NC0125F1W1D0 have been analyzed.

Standard velocity has been 1 mm/min.

It is possible to recognize a similar behaviour for each sample in the linear part.

In the first graph the straight line arrives about to 4000 N, while in the second graph it reaches about 200 MPa.

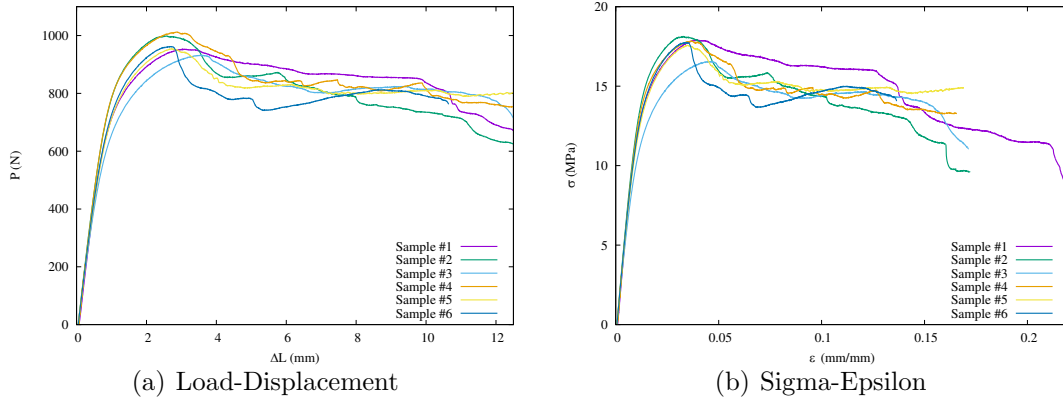


Figure 5.11. Carbon fiber NC0125F4W1D90.

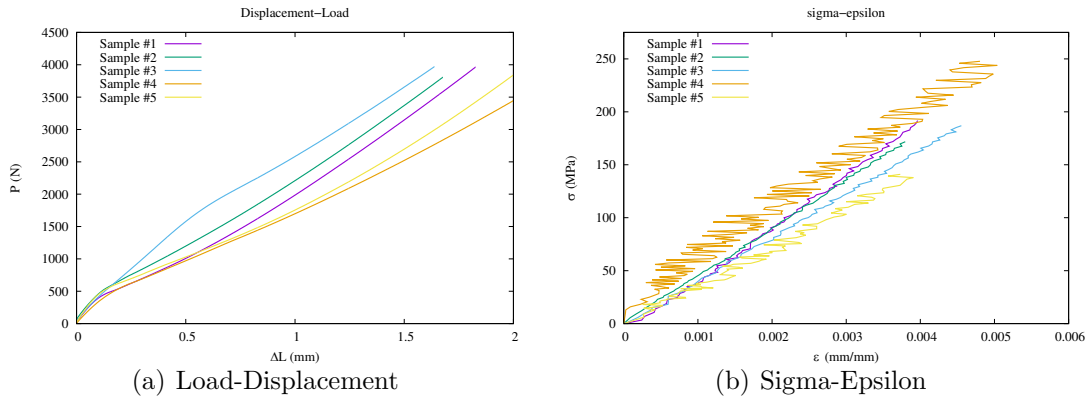


Figure 5.12. Carbon fiber NC0125F1W1D0.

5.1.2 Influence of strain rate

Figure 5.13 shows that 1, 2, 3, 4 and 5 sample of Nylon N02R100F10 have been analyzed.

5mm/min and 50mm/min velocities has been compared.

It is possible to recognize a similar behaviour for each sample in the linear part until 15MPa. The first sample with the a lower velocity shows a lower load, and also a lower stress.

Meanwhile the first sample shows an increase of his curve in the non linear part and it exceeds the others samples with higher velocities.

Figure 5.14 shows that 1, 2, 3, 4 and 5 sample of Nylon N02R50F4 have been analyzed. 5mm/min and 50mm/min velocities has been compared.

It is possible to recognize a similar behaviour for each sample in the linear part until

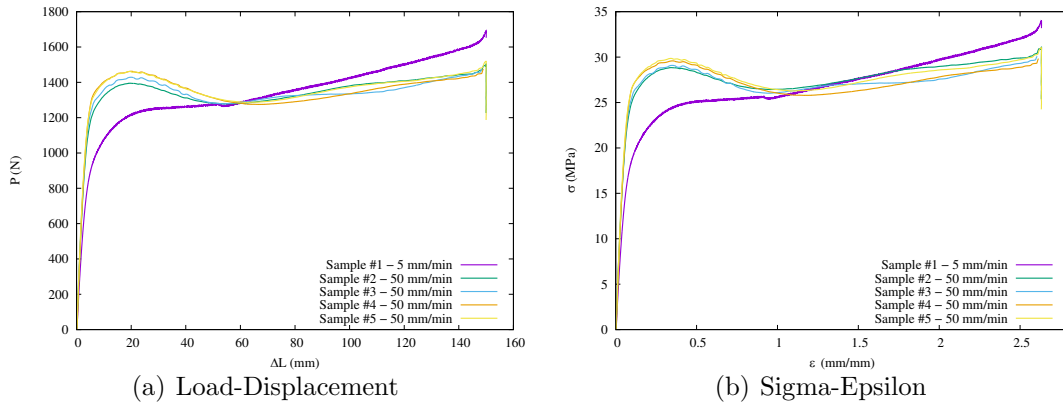


Figure 5.13. Different velocities of Nylon N02R100F10.

10MPa. The first ones samples with the a lower velocity show a lower load, and also a lower stress.

Meanwhile the first ones samples show an increase of his curve in the non linear part and it exceeds the others samples with higher velocities.

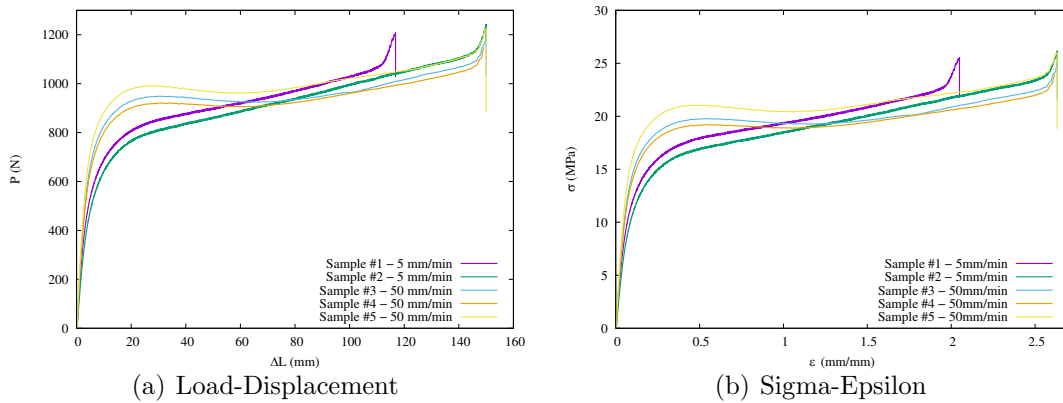


Figure 5.14. Different velocities of Nylon N02R50F4.

Figure 5.15 shows that 1, 2, 3, 4 and 5 sample of Nylon N02H50F4 have been analyzed.

5mm/min and 50mm/min velocities has been compared.

It is possible to recognize a similar behaviour for each sample in the linear part until 5MPa. The second and the third samples with the a higher velocity show a higher load, and also a lower stress.

But the displacement of the samples with higher velocities results lower than the others.

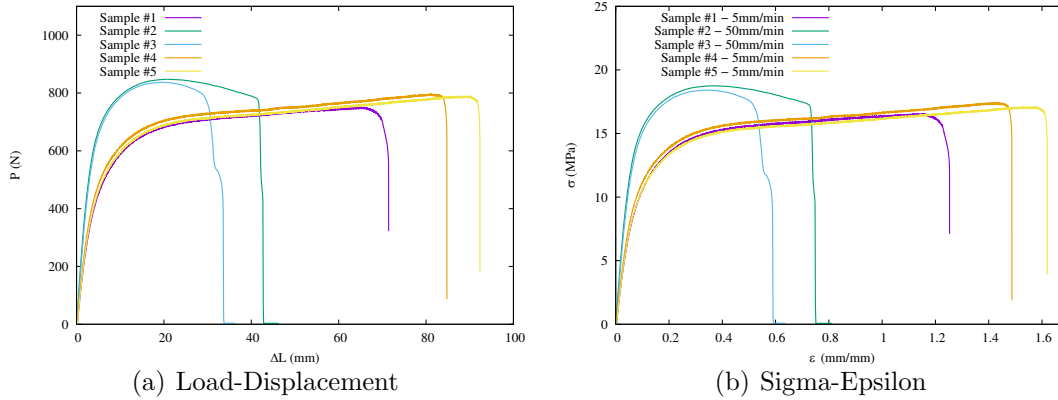


Figure 5.15. Different velocities of Nylon N02H50F4.

5.1.3 Influence of aging

Figure 5.16 shows that 2, 3, 4, 5 and 6 sample of Nylon N02R100F10 have been analyzed.

The oldest samples has been compared to the new one.

It is possible to recognize a similar behaviour for each sample in the linear part until 20MPa.

The sixth sample has completely a different behaviour in the non linear part. In fact it exceeds the other samples in terms of load and stress perceived. It arrives to 1700 N and 37 MPa, meanwhile the oldest samples arrive to 1400 N and about 25 MPa.

Figure 5.17 shows that 3, 4, 5, 6 and 7 sample of Nylon N02R50F4 have been analyzed.

The oldest samples has been compared to the new ones.

It is possible to recognize a similar behaviour for each sample in the linear part until 10MPa.

The sixth and the seventh sample have completely a different behaviour in the non linear part. In fact they exceed the other samples in terms of load and stress perceived. They arrive to 1200 N and 27 MPa, meanwhile the oldest samples arrive to 1000 N and about 20 MPa.

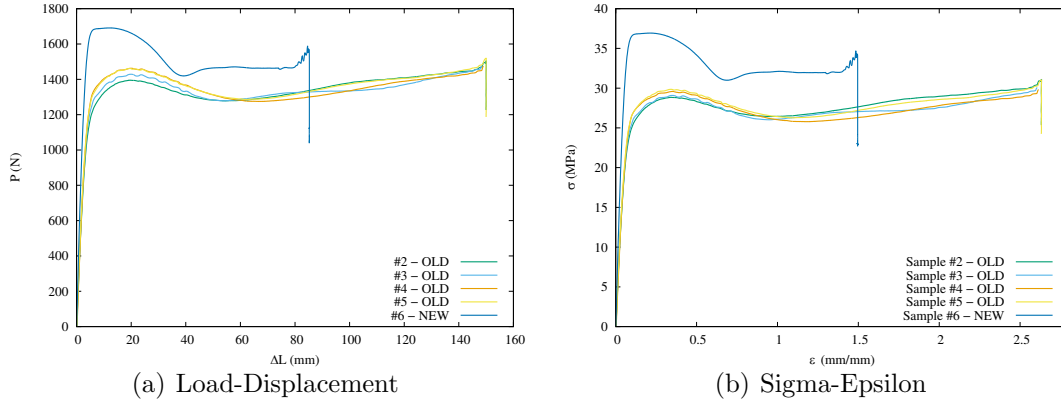


Figure 5.16. Old and new samples of Nylon N02R100F10.

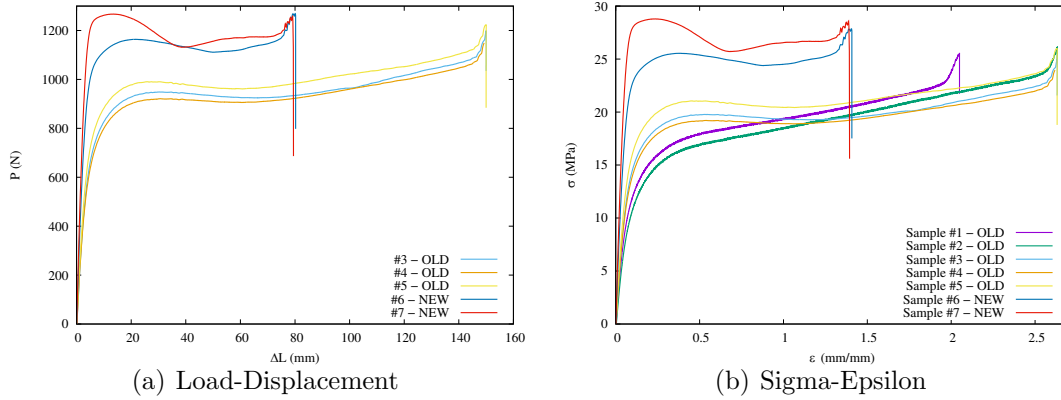


Figure 5.17. Old and new samples of Nylon N02R50F4.

5.2 Young Modulus

Young's modulus, also known as the elastic modulus, is a measure of the stiffness of a solid material. It is a mechanical property of linear elastic solid materials, and will be more or less dependent on temperature, depending on the material being considered. It defines the relationship between stress (force per unit area) and strain (proportional deformation) in a material.

Young's modulus E , can be calculated by dividing the tensile stress by the engineering extensional strain, in the elastic linear portion of the physical stress-strain curve through the equation 5.1:

$$E = \frac{\sigma}{\epsilon} = \frac{F/A}{\Delta L/L_0} \quad (5.1)$$

5.2.1 Nylon

An average value of the Young Modulus has been calculated to compare each lot of samples after the sigma-epsilon analysis. This value has been called E_{Total} for nylon lots.

Table 5.1 shows E_{Total} compared to E_{Total} released by 3D Printer's software, E_{Nylon} , and $E_{honeycomb}$ for each nylon lot of sample.

Sample	3D Printer E_{Total}	E_{Nylon}	$E_{Honeycomb}$	E_{Total}
N02R100F10	940 MPa	898.23 MPa	-	898.23 MPa
N02R50F4	940 MPa	898.23 MPa	108.37 MPa	538.00 MPa
N02H50F4	940 MPa	898.23 MPa	110.85 MPa	539.13 MPa
N02T25F4	940 MPa	898.23 MPa	54.93 MPa	513.63 MPa
N02T50F4	940 MPa	898.23 MPa	102.18 MPa	535.18 MPa
N02T75F4	940 MPa	898.23 MPa	377.65 MPa	660.81 MPa

Table 5.1. Nylon Young's modulus calculation.

Figure 5.18 shows the difference between E_{Total} for each pattern. It is visible how the trend raises up when increasing the density of the internal pattern.

It has been calculated the honeycomb Young modulus through the equation 5.2, thanks to the percentage of density calculated in Table 4.7:

$$E_{honeycomb} = (E_{Total} - E_{Nylon} * \%V_{Nylon}) / \%V_{honeycomb} \quad (5.2)$$

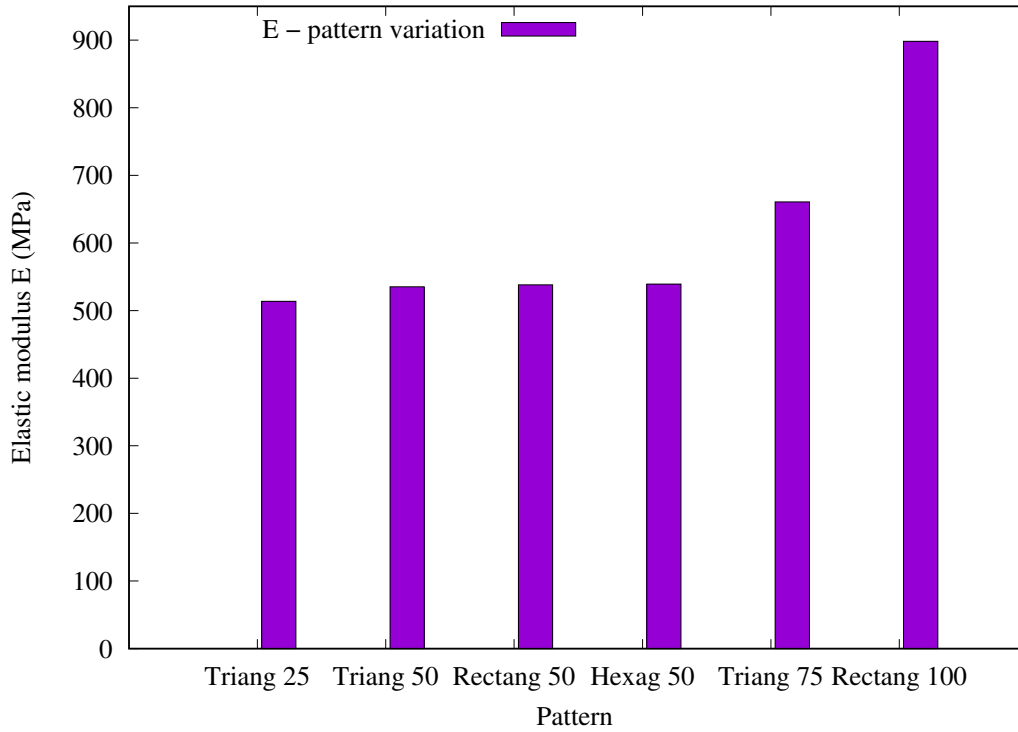
Figure 5.19 shows the polynomial curve that compares different densities to the honeycomb elastic modulus. It is visible how the trend raises up when increasing the density of the internal pattern.

25% of density's lot has 55 MPa of elastic modulus, increasing to about 110 MPa when approaching to 50% of density.

75% of density's lot has 400 MPa of elastic modulus, increasing to about 900 MPa when approaching to 100% of density.

The equation that sets the curve is expressed in equation 5.3:

$$y = 0.0002x^3 + 0.1555x^2 - 10.563x + 218.99 \quad (5.3)$$

Figure 5.18. E_{Total} variation with different patterns.

5.2.2 Carbon fiber

Table 5.2 shows experimental E_{Fiber} compared to E_{Fiber} released by 3D Printer's software, E_{Nylon} , and E_{Total} for each carbon fiber lot of sample.

Sample	3DPrinter	E_{Fiber}	E_{Fiber}	E_{Nylon}	E_{Total}
NC0125F2W1D0	54 GPa	53.59 GPa	0.898 GPa	21.25 GPa	
NC0125F3W2D0	54 GPa	53.64 GPa	0.898 GPa	9.36 GPa	
NC0125F4W1D90		2.37 GPa	0.898 GPa	1.51 GPa	
NC0125F1W1D0	54 GPa	57.64 GPa	0.898 GPa	43.73 GPa	

Table 5.2. Carbon fiber Young's modulus calculation.

Thanks to the percentage of density calculated in the Table 4.8, it has been calculated the carbon fiber Young modulus through 5.4 equation:

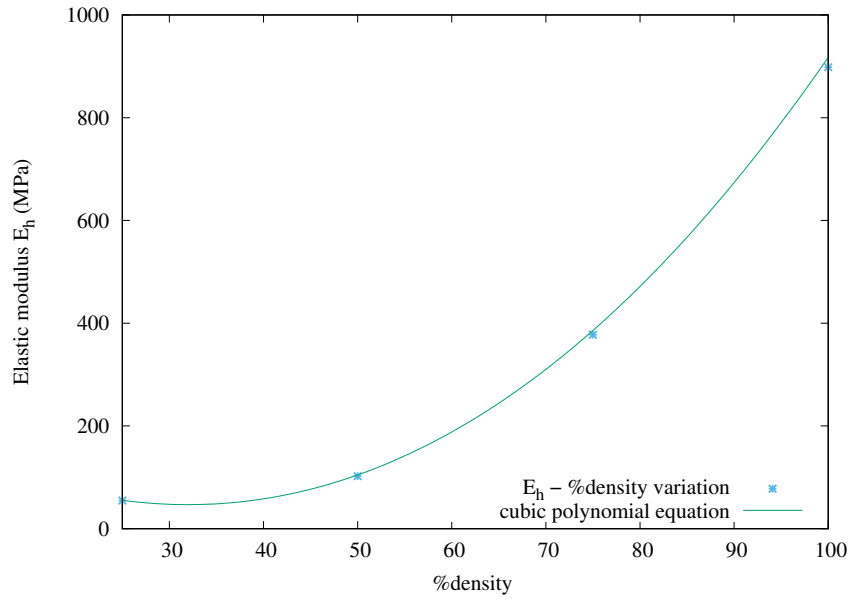


Figure 5.19. E Variation with different density.

$$E_{fiber} = (E_{Total} - E_{Nylon} * \%V_{Nylon}) / \%V_{Fiber} \quad (5.4)$$

The Fig. 5.20 shows how similar has been the measured fibers Young's modulus compared to the fibers Young's modulus given by the 3D Printer.

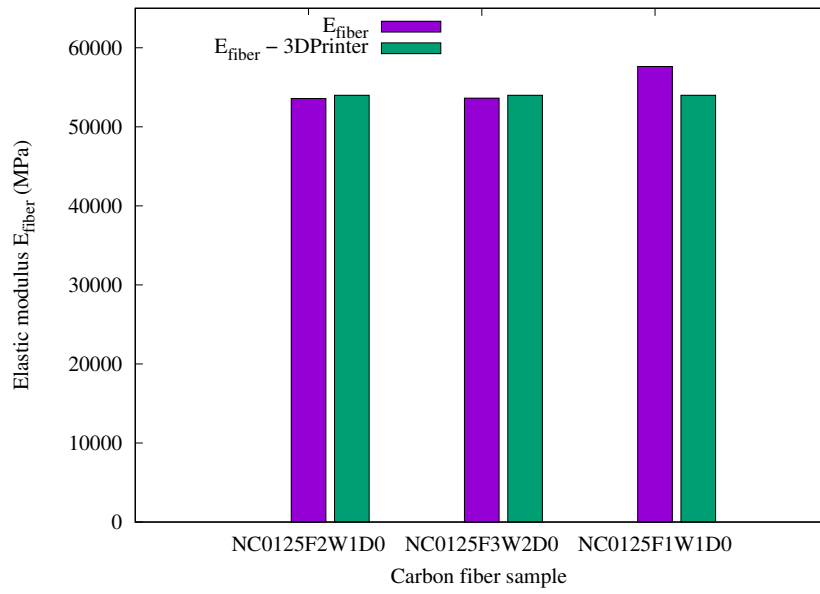


Figure 5.20. Carbon fiber E Variation.

Chapter 6

Three point bending test

In a 3-point bend test, the convex side of the sheet or plate is placed in tension, and the outer fibers are subjected to maximum stress and strain. Failure will occur when the strain or elongation exceeds the material's limits.

ASTM normatives has been respected in order to measure displacements developed on the middle section.

It is important to point out that no samples subjected to stress have been broken because applied load has been restrained.

Fig. 6.1 shows the three-point bending test setup.



Figure 6.1. Three-point bending setup.

The three point bend test is a classical experiment in mechanics, used to measure the Young's modulus of a material in the shape of a beam. The beam, of length L , rests on two roller supports and is subject to a concentrated load P at its centre.

Fig. 6.2 shows a schematic of the three point bend test (top), with graphs of bending moment M , shear Q and deflection w .

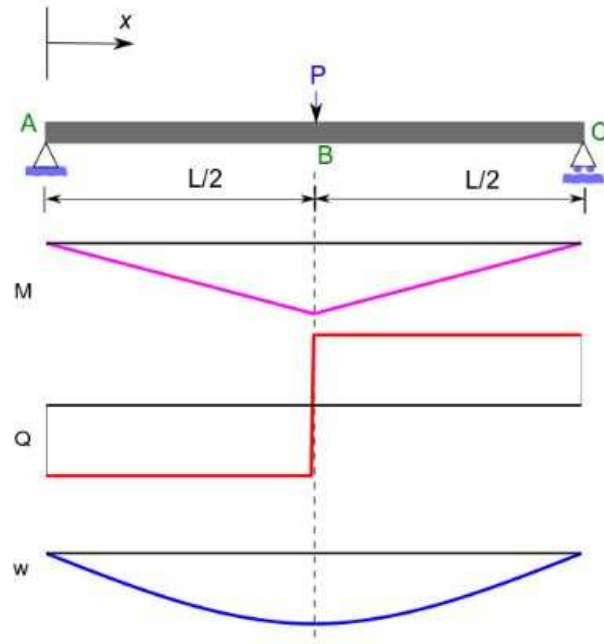


Figure 6.2. Three-point bending setup.

It can be shown that the deflection w_0 at the centre of the beam is:

$$w_0 = \frac{PL^3}{48EI} \quad (6.1)$$

where E is the Young's modulus.

I is the second moment of area defined by:

$$I = \frac{d^3b}{12} \quad (6.2)$$

where d is the beam's depth and b is the beam's width. By measuring the central deflection w_0 and the applied force P , and knowing the geometry of the beam and the experimental apparatus, it is possible to calculate the Young's modulus of the material.

6.1 Sigma-epsilon graphs

Sigma-epsilon graphs are useful to understand the breaking test behaviour.

The output from the testing machine are force and elongation. To find the flexural stiffness and maximum strength the data need to be converted to a stress-strain diagram.

The maximum stress at the outer surface at the midpoint between the supports. This stress can be calculated using equation 3.3.

The maximum strain is on the outer surface in the middle between the two supports. The maximum strain is calculated using equation 3.4.

$$\sigma(max) = \frac{3PL}{2bd^2} [N/m^2] \quad (6.3)$$

$$\epsilon(max) = \frac{6Dd}{L^2} [-] \quad (6.4)$$

Where P is the force, L is the support span, b is the width of the beam, d is the depth and D is the extension.

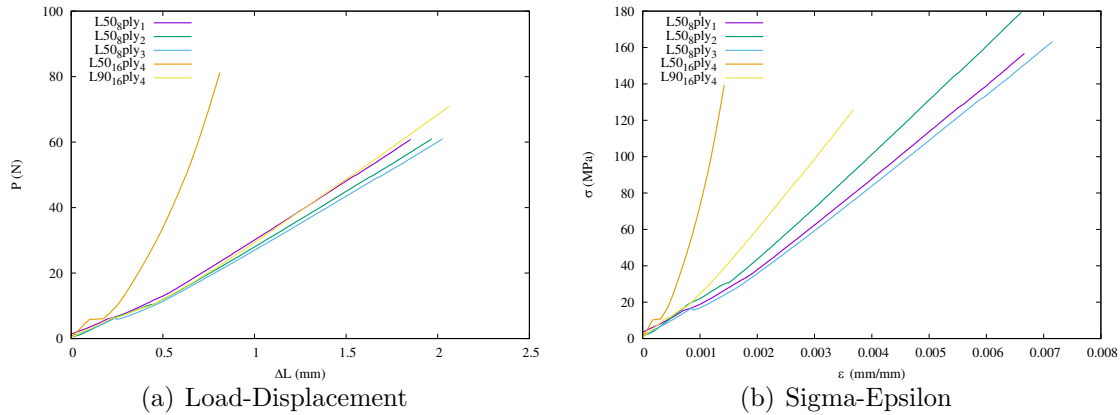


Figure 6.3. Sigma-epsilon graph of carbon fiber samples for 3pb.

Besides three samples renamed "NC0125L50p8F1W1D0", also "NC0125L90p16F1W1D0" lot has been tested considering the span length as 50 mm and 90 mm.

Fig. 6.3 shows sigma-epsilon graph of carbon fiber samples obtained through upper formulation.

It is visible a different behavior of "L50.16ply". It has been solicited with a higher load, and the span length is no longer proportionate to the real length of the sample.

It is clear that the curve is steeper where carbon fiber is more present, in fact

”L90.16ply” has a higher volume percentage of fiber.

Fig. 6.4 shows sigma-epsilon graphs of only carbon fiber have been obtained deleting nylon matrix from samples geometry.

It is visible how the curves are steeper than the previous graphs, caused to the higher elasticity of the fiber.

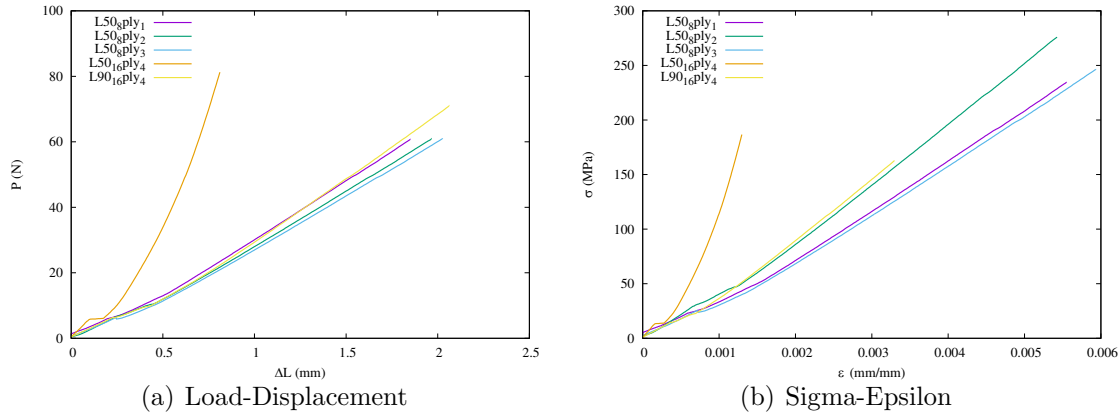


Figure 6.4. Sigma-epsilon graph of only carbon fiber for 3pb.

6.2 Young modulus

The tangent modulus of elasticity, often called the ”modulus of elasticity”, is the ratio, within the elastic limit, of stress to corresponding strain.

It is calculated by drawing a tangent to the steepest initial straight-line portion of the load-deflection curve and using equation 3.5.

$$E = \frac{L^3 m}{4bd^3} [MPa] \quad (6.5)$$

Where:

E = modulus of elasticity in bending, MPa,

L = support span, mm,

b = width of beam tested, mm,

d = depth of beam tested, mm,

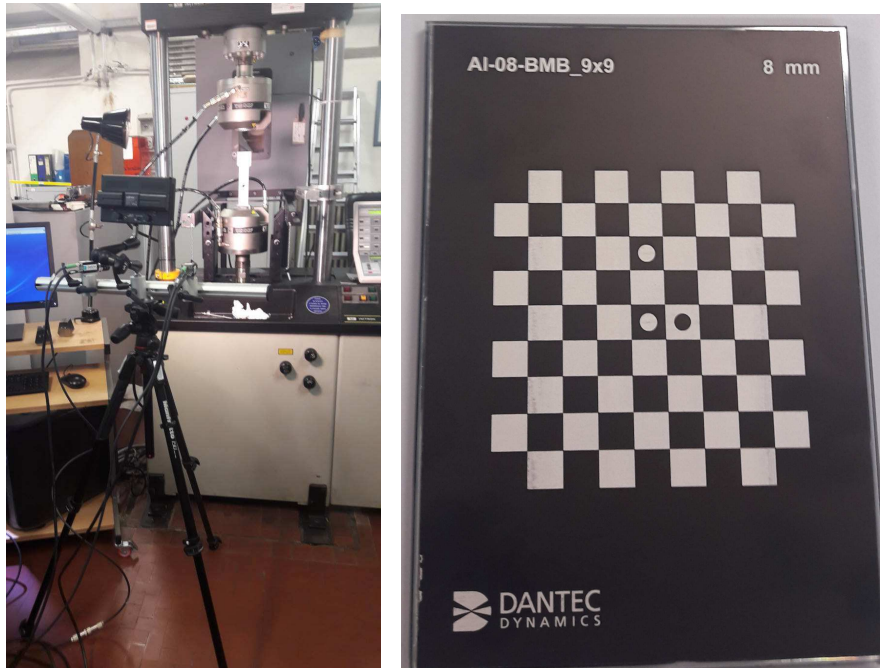
m = slope of the tangent to the initial straight-line portion of the load-deflection curve, N/mm of deflection.

Sample	E (MPa)	E fiber (MPa)	E fiber by printer (MPa)
L50.8ply.1	25615	46043	54000
L50.8ply.2	29574	55492	54000
L50.8ply.3	24887	45282	54000
L90.16ply.4	32108	46366	54000

Table 6.1. Carbon fiber Young's modulus calculation for 3pb.

Chapter 7

Digital image correlation



(a) Cameras setup.

(b) Calibration of cameras.

Figure 7.1. Setup for digital image correlation.

It has been used 'ISTRA 4D Dantec Dynamics' Software for digital image correlation. Before the start of traction test, two cameras have been placed in front of the sample at the same distance. After connecting cameras to electronic and laptop, it has been open live image view icon. Both cameras have been adjusted in the region of interest, so it coincides on the centre of both cameras. Angle between the cameras should be between 40° and 60° .

After checking the frame rate, and setting camera exposure time for each camera, it has been started a new calibration. Through a calibration target given from 'Dantec Dynamics' and shown in Fig. 7.1, it has been setted a new target in the software, filling the image as much as possible.

Starting different acquisitions and giving different names, it has been taken reference shot for each specimen and an image for each step. When correlations failed, a new mask has been created, checking the position of the start point and the evaluation settings. Opening 3D visualization it was been possible to manage different options and view different graphs and figures shown in the next section. X axis follows longitudinal orientation, y axis trasversal orientation.

[26]

7.1 Poisson's ratio and Shear modulus

Poisson's ratio, denoted by the Greek letter 'nu', ν , is the negative of the ratio of transverse strain to axial strain. For small values of these changes, ν is the amount of transversal expansion divided by the amount of axial compression.

Equation 7.1 indicates the Poisson's ratio theoretical formula:

$$\nu = -\frac{\Delta\epsilon_y}{\Delta\epsilon_x} \quad (7.1)$$

Where:

ν = Poisson's ratio;

$\Delta \epsilon_y$ = difference between displacements long y axis;

$\Delta \epsilon_x$ = difference between displacements long x axis.

The shear modulus is one of several quantities for measuring the stiffness of materials.

The shear modulus is concerned with the deformation of a solid when it experiences a force parallel to one of its surfaces while its opposite face experiences an opposing force. In the case of an object shaped like a rectangular prism, it will deform into a parallelepiped like in Fig. 7.2

One possible definition of a fluid would be a material with zero shear modulus.

In materials science, shear modulus or modulus of rigidity, denoted by G , is defined as the ratio of shear stress to the shear strain:

$$G = \frac{\tau_{xy}}{\gamma_{xy}} = \frac{F/A}{\Delta x/l} = \frac{Fl}{A\Delta x} \quad (7.2)$$

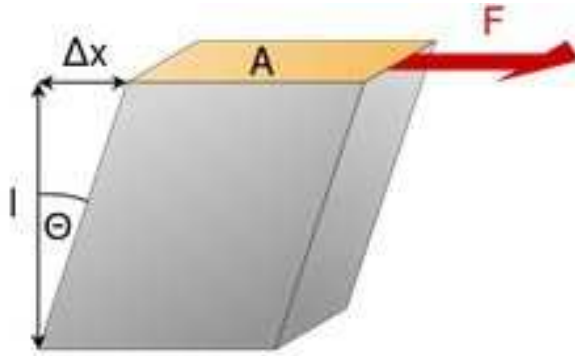


Figure 7.2. G modulus.

Where:

$$\tau_{xy} = \frac{F}{A} = \text{shear stress};$$

F = force which acts;

A = area on which the force acts;

γ_{xy} = shear strain;

Δx = transverse displacement;

l = initial length.

7.1.1 Nylon

Table 7.1 indicates Poisson's ratio, Young modulus, and Shear modulus for each nylon sample analyzed.

Equation 7.3 has been used to find the values in the following table.

$$G = \frac{E}{2(1 + \nu)} \quad (7.3)$$

Sample	ν	E (MPa)	G (MPa)
N02R100F10.3	0.3944	840.82	301.50
N02R100F10.4	0.3882	863.12	310.88
N02R100F10.5	0.3620	957.81	351.62
N02T25F4.5	0.4223	513.63	180.56
N02T75F4.5	0.4092	660.81	234.46

Table 7.1. Poisson's ratio and Shear modulus of nylon samples.

Thanks to 3D visualization it has been possible to visualize graphs like 'Displacement long x or y direction', 'Tangential strain long x or y direction', 'Standard deviation of strain long x or y direction', 'Lagrange tangential strain long x or y direction' and other engineering parameters.

In this section is described for each batch of nylon samples analyzed how Poisson's ratio has been calculated, are showed before-after photos of the samples during testing, and tangential strain graphs.

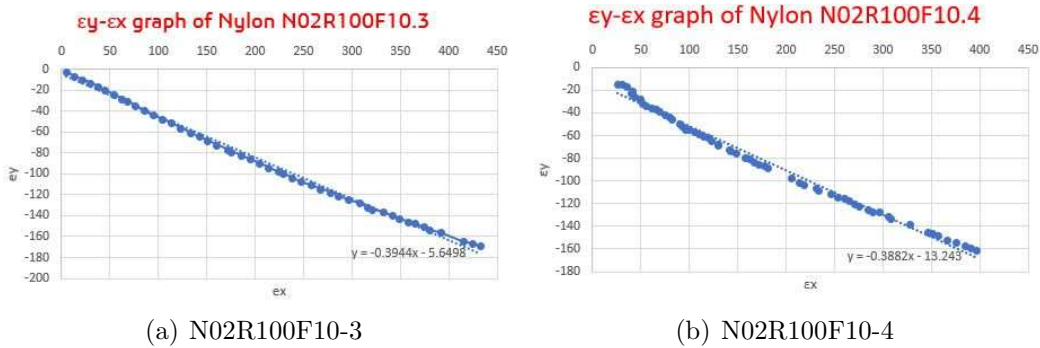


Figure 7.3. $\epsilon_y - \epsilon_x$ graph of third and fourth Nylon N02R100F10 sample.

A linear polynomial equation it has been calculated from the $\epsilon_y - \epsilon_x$ graph for each nylon sample.

The derivative of the straight line is the average of Poisson's number and it is represented in Figure 7.3 for Nylon N02R100F10.3 and N02R100F10.4.

The average value of Poisson's number for Nylon N02R100F10.3 is 0.3944, for N02R100F10.4 is 0.3882.

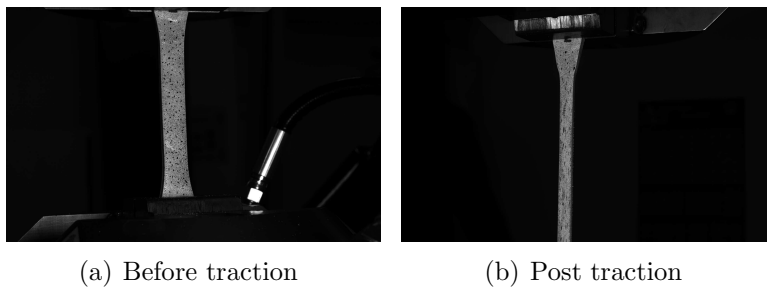
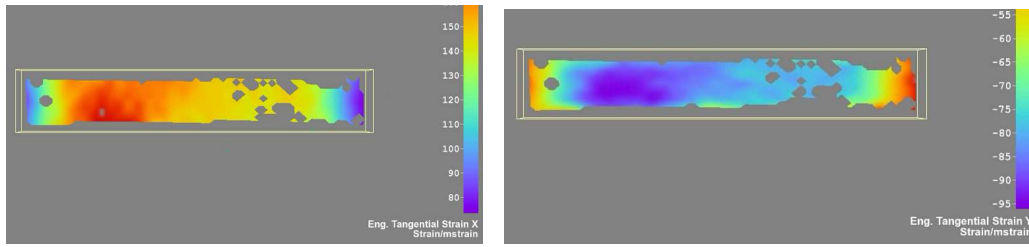


Figure 7.4. Photo of Nylon N02R100F10.3 before and after traction.

Figure 7.4 shows photos of the N02R100F10 third sample before and after traction test. This lot of samples did not break, but his elongation is visible.

One final step of tangential strain long x and y axis is taken during the break phase. Figure 7.5 shows both of the graphs, presenting also the scale in mstrain on the right.

It is visible how tangential strain is higher long x axis and lower long y axis.



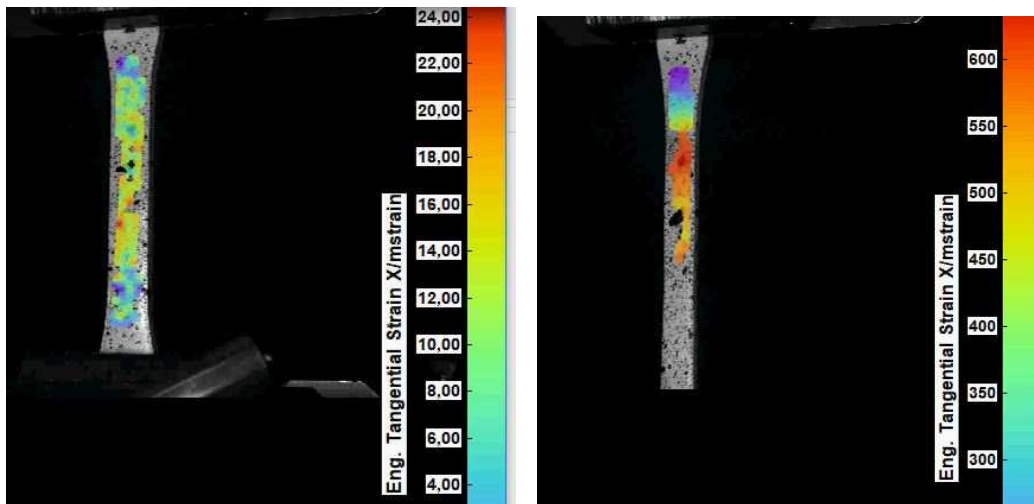
(a) Tangential strain long x axis

(b) Tangential strain long y axis

Figure 7.5. Tangential Strain for nylon N02R100F10.3.

In order to take one initial and one final step of tangential strain long x axis it is shown nylon N02R100F10.4.

Figure 7.6 shows both of the photos, presenting also the scale in mstrain on the right. It is visible how tangential strain long x axis is higher during post traction. Red colour shows high level of mstrain.



(a) Before traction

(b) Post traction

Figure 7.6. Tangential Strain long x axis for Nylon N02R100F10.4.

The derivative of the straight line is the average of Poisson's number and it is represented in Figure 7.7 for Nylon N02T25F4.5 and N02T75F4.5. The average

value of Poisson's number for Nylon N02T25F4.5 is 0.4223, for Nylon N02T75F4.5 is 0.4092.

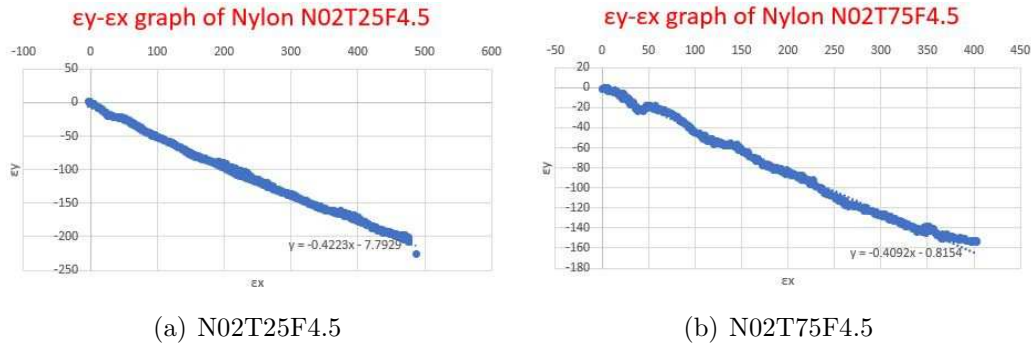


Figure 7.7. $\epsilon_y - \epsilon_x$ graph of the fifth Nylon N02T25F4 and N02T25F4 sample.

Figure 7.8 shows photos of the N02T25F4 fifth sample before and after traction test. This batches of samples did break.

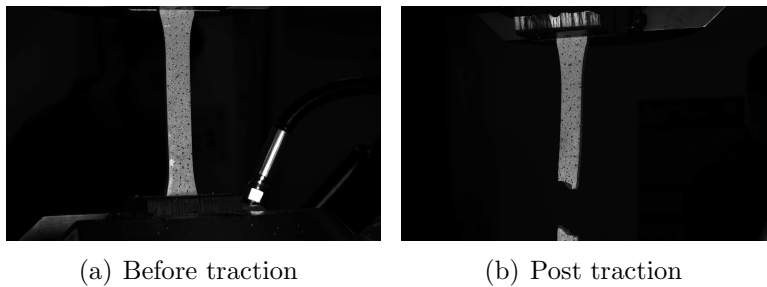


Figure 7.8. Photo of Nylon N02T25F4.5 before and after traction.

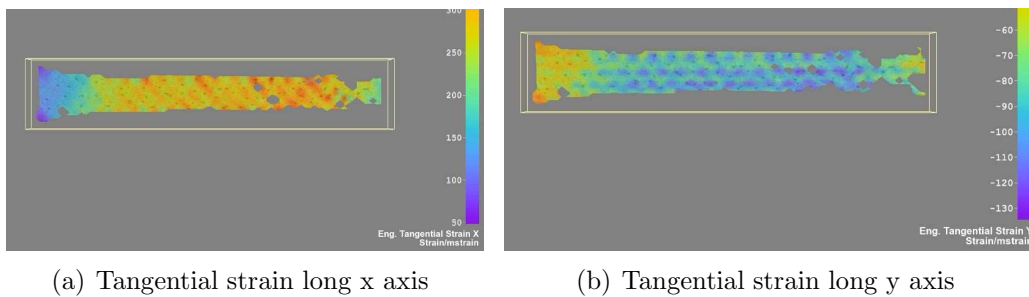


Figure 7.9. Tangential Strain for N02T25F4.5.

One final step of tangential strain long x and y axis is taken during the break phase.

Figure 7.9 shows both of the graphs, presenting also the scale in mstrain on the right. It is visible how tangential strain is higher long x axis and lower long y axis.

7.1.2 Carbon Fiber

In this subsection the experimental characterization of polymer matrix and polymer based carbon fiber reinforced composite laminate by employing a whole field non-contact digital image correlation (DIC) technique is presented.

The properties are evaluated based on full field data obtained from DIC measurements by performing a series of tests as per ASTM standards.

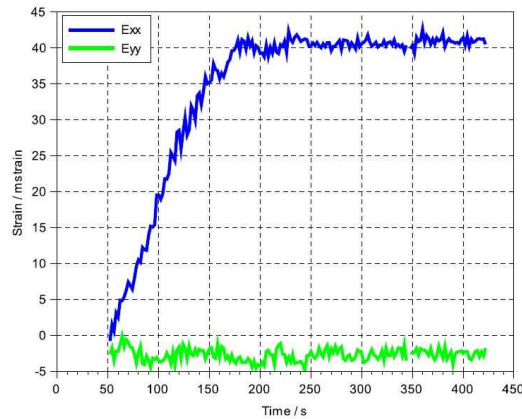


Figure 7.10. Strain vs time.

The aspect ratio of region of interest (ROI) chosen for correlation should be the same as that of camera resolution aspect ratio for better correlation.

In this subsection it is described for each lot of carbon fiber samples analyzed how Poisson's ratio has been calculated, are showed before-after photos of the samples during testing, and tangential strain graphs.

Fig. 7.10 is an output example released by the software used to digital correlation of strain during time. All the outputs have been reworked.

Table 7.2 indicates Poisson's ratio, Young modulus, and Shear modulus for each carbon fiber sample analyzed.

Sample	ν	E (MPa)	G (MPa)
NC0125F2W1D0.1	0.4462	21623.85	7476.09
NC0125F4W1D90.1	0.0141	1552.34	765.38
NC0125F3W2D0.1	0.4176	9378.36	3307.83
NC0125F1W1D0.1	0.3807	50210	18182.81
NC0125F1W1D0.2	0.3817	44941	16262.94
NC0125F1W1D0.3	0.5184	41333	13610.71
NC0125F1W1D0.4	0.6473	46438	14095.19
NC0125F1W1D0.5	0.6218	35738	11018.00

Table 7.2. Poisson's ratio and Shear modulus of carbon fiber samples.

A linear polynomial equation it has been calculated from the $\epsilon_y - \epsilon_x$ graph for each carbon fiber sample.

The derivative of the straight line is the average of Poisson's number and it is represented in Figure 7.11 for Carbon Fiber NC0125F2W1D0.1 and NC0125F3W2D0.1.

The average value of Poisson's number for Carbon Fiber NC0125F2W1D0.1 is 0.4462, for Carbon Fiber NC0125F3W2D0.1 is 0.4176.

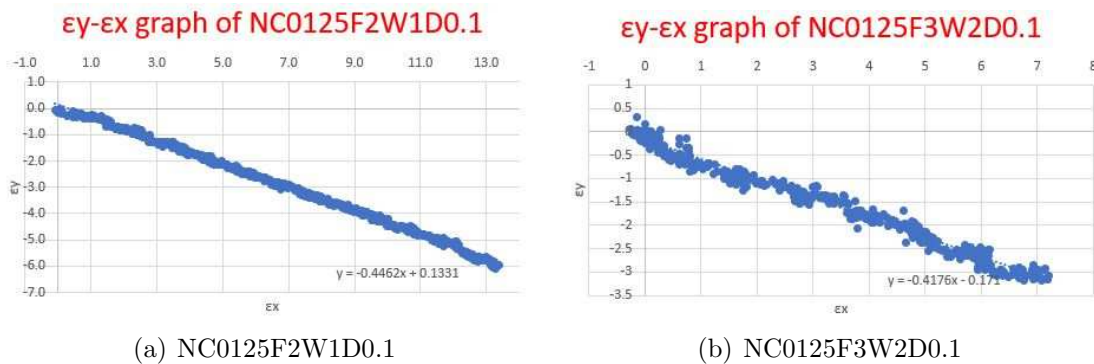


Figure 7.11. $\epsilon_y - \epsilon_x$ graph of NC0125F2W1D0.1 and NC0125F3W2D0.1.

Figure 7.12 shows photos of the NC0125F2W1D0 first sample before and after traction test. It is visible how the white paint has been lost during the break.

Figure 7.13 shows photos of the NC0125F4W1D90 first sample before and after traction test. One final step of tangential strain long x and y axis is taken during the break phase.

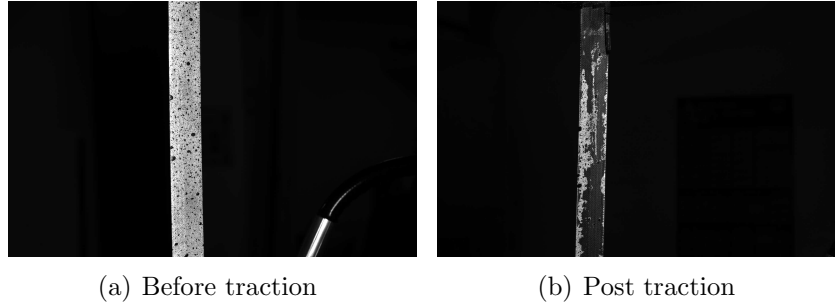


Figure 7.12. Photo of Carbon Fiber NC0125F2W1D0.1 before and after traction.

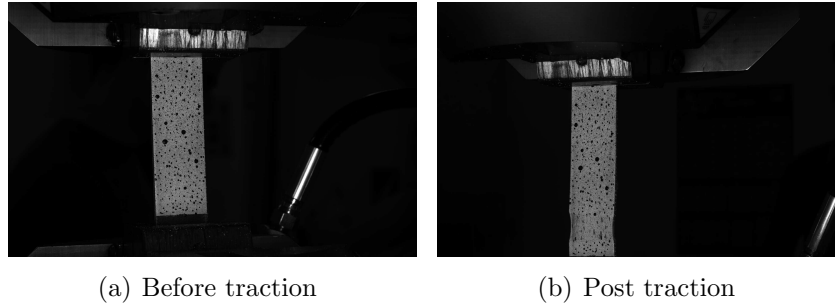


Figure 7.13. Photo of Carbon Fiber NC0125F4W1D90.1 before and after traction.

Figure 7.14 represents $\epsilon_y - \epsilon_x$ graph of Carbon fiber NC0125F4W1D90.1. The average value of Poisson's number for Carbon fiber NC0125F4W1D90.1 is 0.0141.

Figure 7.15 shows both of the graphs, presenting also the scale in mstrain on the right. It is visible how tangential strain is higher long x axis and lower long y axis.

Figure 7.16 represents " ϵ_x - steps" graph of Carbon fiber NC0125F1W1D0.3, presenting also an adimensional scale on the right.

It is visible how the correlation has been successful where points have not been done too big. It has been indentified a local region of interest (ROI) in which the correlation worked better. It is clear that the values range is from 0.002 to 0.004.

Figure 7.17 represents " ν - steps" graph of Carbon fiber NC0125F1W1D0.1. The average value of Poisson's number for Carbon fiber NC0125F1W1D0.1 is 0.38.

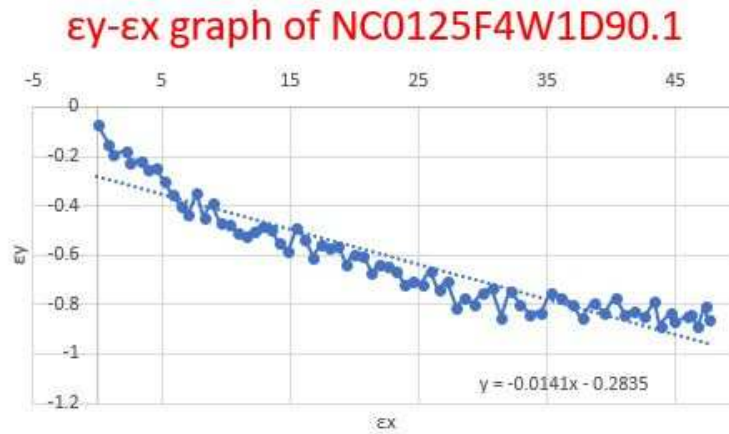
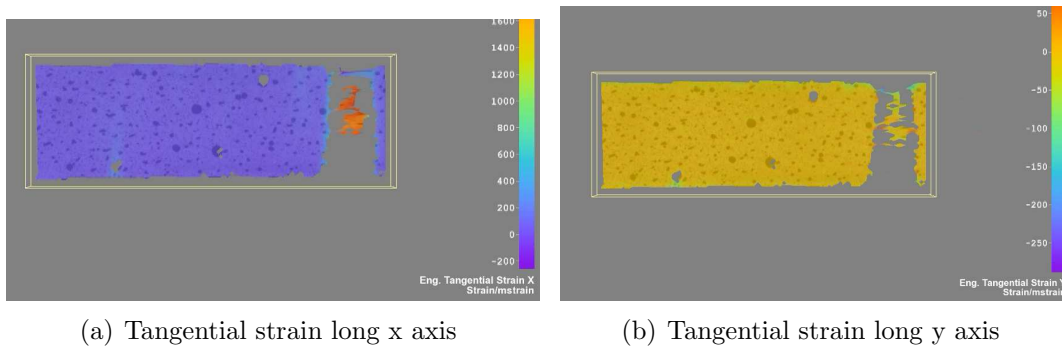


Figure 7.14. $\epsilon_y - \epsilon_x$ graph of Carbon Fiber NC0125F4W1D90.1.



(a) Tangential strain long x axis

(b) Tangential strain long y axis

Figure 7.15. Tangential Strain for NC0125F4W1D90.1.



Figure 7.16. NC0125F1W1D0.3 ϵ_x graph.

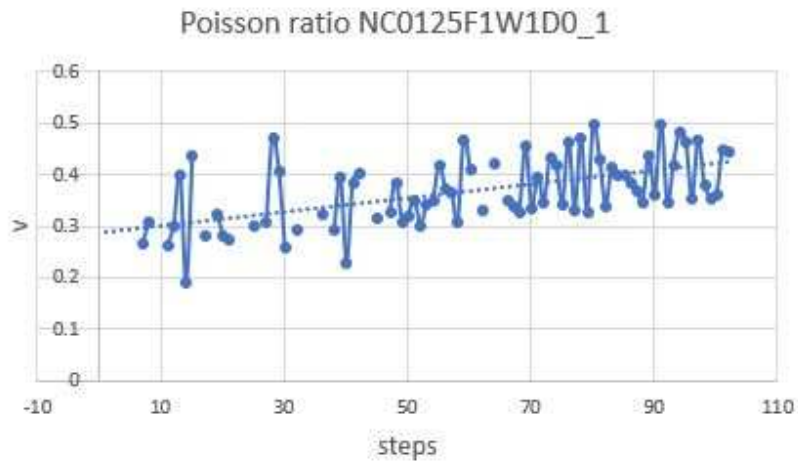


Figure 7.17. NC0125F1W1D0 Poisson's ratio.

Chapter 8

Conclusions

The results of this work have shown that digital image correlation is a valid system to measure strains and it is certainly an effective method to calculate the Poisson's ratio and the shear modulus.

Despite the software Eiger does not allow to compare Poisson's ratio, the results found in this thesis were particularly consistent compared to related composite materials.

As regards instead Young's modulus of 3D printed and tested samples, it is really similar to the value given by datasheet.

Furthermore it is clear that the strain rate and the aging effects are really considerable and it is desirable to investigate better their behavior in the future.

In this thesis water cutter jetting has been used to cut the carbon fiber plate and to obtain different specimens. Final result has not been positive because two nylon's layers have not been sufficient to counter the water jet. In this case this machine is not recommended for cutting this types of materials.

In the final analysis it has been noticed that Young's modulus for three point bending tests is slightly smaller than Young's modulus measured for traction tests.

Bibliography

- [1] B. Berman, “3-D printing: The new industrial revolution” in *Hofstra University NY, USA*, 2011.
- [2] H. Bikas, P. Stavropoulos, G. Chryssolouris, “Additive manufacturing methods and modelling approaches: a critical review” in *University of Patras, Greece*, 2015.
- [3] H. Dirk, J. Lukaszewicz, C. Ward, K. D. Potter, “The engineering aspects of automated prepreg layup: history, present and future” in *University of Bristol, UK*, 2011.
- [4] K. V. Wong, A. Hernandez, “A Review of Additive Manufacturing” in *Department of Mechanical and Aerospace Engineering, University of Miami, FL, USA*, 2012.
- [5] F. Ning, W. Cong, J. Qiu, J. Wei, S. Wang, “Additive manufacturing of carbon fiber reinforced thermoplastic composites using fused deposition modeling” in *Department of Industrial Engineering, Texas, USA*, 2015.
- [6] A. Haavajoe, M. Mikola, M. Pohlak, “Design and manufacturing of variable angle tow laminate” in *Department of Machinery, Tallinn, Estonia*.
- [7] B. Kim, P. Weaver, K. Potter, “Computer aided modelling of variable angle tow composites manufactured by continuous tow shearing” in *ACCIS (Advanced Composite Centre for Innovation and Science), University of Bristol, UK*, 2015.
- [8] —, “Manufacturing characteristics of the continuous tow shearing method for manufacturing of variable angle tow composites” in *University of Bristol, UK*, 2014.
- [9] G. Raju, P. Weaver, Z. Wu, “Buckling and postbuckling of variable angle tow composite plates under in-plane shear loading” in *University of Walk, UK*, 2014.
- [10] B. Kim, P. Weaver, K. Potter, “Continuous tow shearing for manufacturing variable angle tow composites” in *University of Bristol, UK*, 2012.
- [11] G. Raju, P. Weaver, Z. Wu, “Postbuckling analysis of variable angle tow composite plates” in *University of Walk, UK*, 2013.
- [12] B. Kim, K. Hazra, P. Weaver, K. Potter, “Limitations of fibre placement techniques for variable angle tow composites and their process-induced defects” in *University of Bristol, UK*, 2011.

- [13] H. Bansemir, O. Haider, “Fibre composite structures for space applications, recent and future developments” in *Munich, Germany*, 1997.
- [14] G. Nannan, M. Leu, “Additive manufacturing: technology, applications and research needs” in *Missouri University of Science and Technology, USA*, 2013.
- [15] in “ASTM D790-17 - Standard Test Methods for Flexural Properties of Unreinforced and Reinforced Plastics” 2017.
- [16] in “ASTM D2344-06 - Short-beam strength of polymer matrix composite materials and their laminates” 2006.
- [17] in “ASTM D3039-17 - Tensile Properties of Polymer Matrix Composite Materials” 2017.
- [18] A. Mehar, S. Ahmed, G. Kumar, “Experimental Investigation and FE Analysis of CFRP Composites” in *M.J. College of Engineering and Technology*, 2015.
- [19] A. Forster, “Materials Testing Standards for Additive Manufacturing of Polymer Materials: State of the Art and Standards Applicability” in *National Institute of Standards and Technology, U.S. Department of Commerce*, 2015.
- [20] G. Melenka, B. Cheung, J. Schofield, M. Dawson, J. Carey, “Evaluation and prediction of the tensile properties of continuous fiber-reinforced 3D printed structures” in *Mechanical Engineering, University of Alberta, Edmonton, Canada*, 2016.
- [21] G. Goh, V. Dikshit, S. Agarwala, S. Sing, J. Wei, “Characterization of mechanical properties and fracture mode of additively manufactured carbon fiber and glass fiber reinforced thermoplastics” in *Singapore Centre for 3D Printing, Nanyang Technological University, Singapore*, 2017.
- [22] G. Engkvist, “Investigation of microstructure and mechanical properties of 3D printed Nylon” in *Department of Engineering Sciences and Mathematics, Lulea University of Technology*, 2017.
- [23] F. Ning, W. Cong, Y. Hu, H. Wang, “Additive manufacturing of carbon fiber-reinforced plastic composites using fused deposition modeling: Effects of process parameters on tensile properties” in *Department of Industrial Engineering, Texas Tech University, TX, USA*, 2016.
- [24] P. Parandoush, D. Lin, “A review on additive manufacturing of polymer-fiber composites” in *Department of Industrial and Manufacturing Systems Engineering, Kansas State University, Manhattan, USA*, 2017.
- [25] J. Lewicki, J. Rodriguez, C. Zhu, “3D-Printing of Meso-structurally Ordered Carbon Fiber/Polymer Composites with Unprecedented Orthotropic Physical Properties” in *Scientific Reports, www.nature.com/scientificreports*, 2017.
- [26] M. Kashfuddoja, R. Prasath, M. Ramji, “Study on experimental characterization of carbon fiber reinforced polymer panel using digital image correlation: A sensitivity analysis” in *Engineering OpticsLab, Department of Mechanical Engineering, Yeddumailaram, India*, 2014.